Department of Physics and Astronomy
University of Heidelberg

Bachelor Thesis in Physics
submitted by

Michael Rudolf Ciupek

born in Landstuhl (Germany)

2016

Electron identification in different colliding systems with ALICE

This Bachelor Thesis has been carried out by Michael Rudolf Ciupek at the
Physikalisches Institut in Heidelberg
under the supervision of
Priv.-Doz. Dr. Silvia Masciocchi

Abstract

Its important for HFE analysis to know the electron purity for a given electron sample. In this thesis an estimation of the electron purity in an electron sample is given with different detectors of ALICE in Pb- Pb and pp collisions. First of all, the electron purity and hadron contamination of an electron sample, taken from Pb- Pb collisions at $\sqrt{s_{NN}} = 2.76 \ TeV$ and $\sqrt{s_{NN}} = 5.02 \ TeV$, are estimated. Particles contributing to the dE/dx distribution of the electron sample will be described via two different fit models. The first method uses templates, extracted directly from measured TPC dE/dx signals of the hadrons, where as the second method uses different functions to parametrise the different particle contributions. Electron purities obtained by both methods and center of mass energies are put in comparison to each other.

In the second part of this thesis the electron purity of an electron sample, obtained from pp collisions at $\sqrt{s} = 2.76 \ TeV$, and the efficiency of different PID cuts are investigated are investigated with the TPC and EMCal detector. and compared to each other for a large momentum region. In addition the trigger efficiency between the minimum bias and EMCal trigger data was estimated.

Zusammenfassung

Für HFE Analysen ist es wichtig zu wissen, wie rein ein gegebener Datensatz von Elektronen ist. Das Ziel dieser Arbeit besteht in der Abschätzung der Reinheit eines Datensatzes von Elektronen, der aus Pb- Pb oder pp Kollisionen extrahiert wurde, mit verschiedene Detektoren des ALICE Experimentes. Im ersten Teil dieser Arbeit wird die Reinheit von Elektronen und der hadronische Untergrund eines Datensatzes von Elektronen, der in Pb Pb Kollisionen bei einer Schwerpunktsenergie von 2.76 TeV und 5.02 TeV entstanden ist, bestimmt. Teilchen die zur TPC dE/dx Verteilung der Elektronen beitragen werden mithilfe zwei verschiedener Modelle beschrieben. Das erste Modell beschreibt die Teilchen mithilfe von Templates, die direkt von den gemessenen TPC dE/dx Verteilungen der verschiedenen Teilchen extrahiert werden, das zweite Modell hingegen beschreibt Teilchen mithilfe verschiedener Funktionen. Die durch beide Methoden und für beide Schwerpunktsenergien erhaltene Reinheit der Elektronen werden miteinander verglichen.

Der zweite Teil dieser Arbeit befasst sich mit der Abschätzung der Reinheit von Elektronen eines Datensatzes, extrahiert aus pp Kollisionen bei $\sqrt{s} = 2.76 \, TeV$, und der Effizienzs für verschiedene Selektionskriterien mit TPC und EMCal Detektor. Diese verschiedenen Selektionskriterien, wiederum werden in einem weiten Impulsbereich miteinander verglichen. Außerdem soll eine Abschätzung für die Trigger Effizienz zwischen minimum bias und EMCal Trigger gegeben werden.

Contents

1 Introduction

ALICE (A Large Ion Collider Experiment) at the LHC (Large Hadron Collider) at CERN is exploring a state of strongly interacting matter of high density and temperature created in Pb-Pb collisions. This state of matter is called quark- gluon plasma (QGP) and is expected to have occurred few $10^{-6}\mu s$ after the big bang. Therefore, investigating the QGP may help to understand the early evolution of the universe. Moreover, it will lead to an improvement of our understanding of the quantum chromo dynamics (QCD).

Since the QGP can not be measured directly, different observables are needed to investigate the properties of the high density medium. Heavy flavour hadrons containing b- and c- quarks are one possibly approach to explore the medium, since they are created before the formation of the QGP due to their large mass. One possible strategy to analyse heavy flavour hadrons is the measurement of electrons from decays of heavy flavour hadrons. Therefore, it´s important for the analysis of heavy favour hadron decay electrons (HFE) to know how much the electron candidates are contaminated by hadrons. The electron spectrum obtained in this procedure has to be cleaned up from electrons from other decay channels (e. g Darlitz decay) in order to obtain a spectrum of electrons from heavy flavour decays. One technique is the Cocktail method which is explained more detailed in [1]. Therefore, its crucial for heavy flavour hadron decay electron analysis to know how strong the electron candidates are contaminated by other particles.

The aim of this thesis is to show methods to estimate the purity of a given electron sample in different colliding systems. In the first section the QGP and heavy flavour decay electrons as probe of the QGP are described. The second section gives an introduction to the detectors used in this analysis. Section 3 contains the description of different fit models to estimate the electron purity in Pb-Pb collisions at $\sqrt{s_{NN}} = 2.76$ *TeV* recorded in the year 2011. In section 4 an outlook is given for the analysis

of Pb-Pb collisions at $\sqrt{s_{NN}} = 5.02$ *TeV* recorded in 2015. Section 5 will describe electron identification with the TPC and EMCal in proton-proton (pp) collisions at $\sqrt{s} = 2.76$ *TeV*.
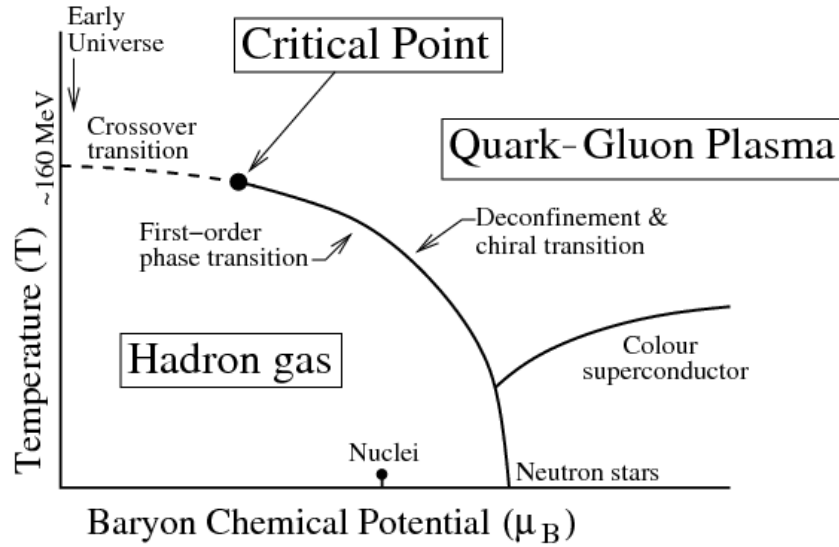
1.1 Quark-Gluon Plasma

Figure 1.1: Phase diagram of QCD. Picture taken from [2].

Quantum chromo dynamics predicts that at high temperature there will be a transition from ordinary nuclear matter to a matter of free and deconfinded quarks and gluons, the so called quark-gluon plasma [3]. Fig. 1.1 shows the phase diagram of QCD as function of the temperature T and the baryon chemical potential μ_B. It shows the different states of strongly interacting matter and the boundary between ordinary nuclear matter and the quark-gluon plasma.

Lattice calculations of quantum chromo dynamics predict the transition, from ordinary hadronic matter to the QGP, to occur at a critical temperature of $T_c \approx 155$ MeV [4], which aggrees well within the systematic uncertainties with data taken of Pb-Pb collisions in 2011 [5].

The quark-gluon plasma is expected to be produced at the LHC in Pb-Pb collisions and has a very short lifetime of around 10-20 fm/c based on models and data comparison [6]. After the creation, the QGP will start to expand. During this expansion it will cool down until it drops under the critical temperature and undergoes a phase transition to form new hadronic matter.

1.2 Heavy Quarks in the QGP

Since the QGP cannot be measured directly at the LHC probes are needed to study the properties of the hot dense medium. Heavy quarks (i.e. charm and beauty) are excellent samples to study the properties of the quark-gluon plasma. Due to their large masses heavy quarks are produced in the initial partonic scattering process during the early stage of the collision. The time scale of production is approximatly $t \approx \frac{1}{2m}$, where m corresponds to the mass of the heavy quark. Therefore, heavy quarks are created even before the formation of the QGP and will experience its full evolution while traversing the medium [1] [7]. The heavy quarks will interact with the medium and loose their energy through gluon emission and scattering processes with the partons in the medium [8].

Measurements of the property of the QGP are done via comparison of heavy flavour observables measured in Pb-Pb collisions where the QGP is formed and interacts with the heavy flavour quarks with a system where the QGP is not supposed to be formed, namly pp collisions [1]. Furthermore, measurments of heavy quark productions in pp collisions provide a testing ground for pertubative quantum chromo dynamics (pQCD) like the Fixed Order calculations with Next-to-Leading-Log resummation (FONLL) and the General Mass Variable-Flavor-Numbering Scheme (GM-VFNS) [7].

Measurements of heavy quarks are done by detecting hadrons containing heavy quarks. One way to study heavy flavour hadrons can be accomplished through measuring electrons and muons from semi- leptonic decays. The branching ratio of semi leptonic decays is on the order of 10% for hadrons containing heavy flavour quarks [9]. A downside in the analysis of semi leptonic decays is the fact, that since neutrinos are produced in semi leptonic decays a full reconstruction of the heavy hadron momentum is impossible.

2 The ALICE Detector

ALICE [10] is an experiment at the LHC [11] which is designed to address the physics of strongly interacting matter and the quark-gluon plasma at extreme values of energy density and temperature in nucleus-nucleus collisions [10]. ALICE overall dimensions are 16 x 16 x 26 m^3 and its total weight is 10.000 t. The detector consists of a central barrel part, which covers the pseudorapidity region of $-0.9 < \eta < 0.9$ over the full azimuth, and a forward muon spectrometer coverin the pseudopapidity of $-4.0 < \eta < -2.5$. The central barrel is embedded in a large solenoid magnet with a magnetic field strength of B = 0.5 T and measures signals of hadrons, electrons and photons, whereas the forward muon spectrometer was designed to measure quarkonia states.

Fig. 2.1 shows the ALICE apparatus with its different sub detectors.
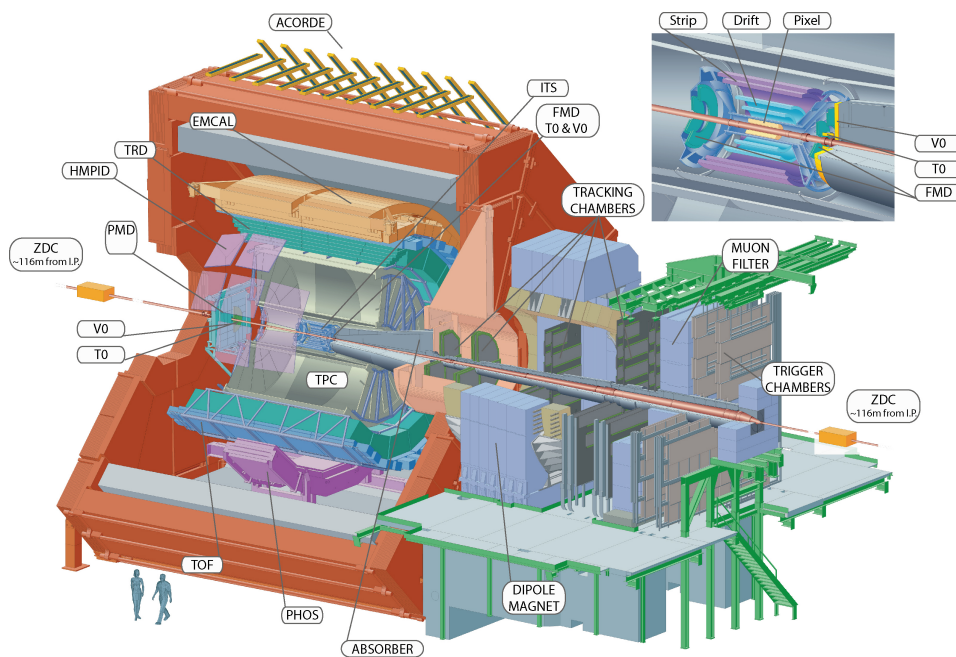

Figure 2.1: Schematic view on ALICE with its different sub detectors[3]

The central barrel contains from the beamline to the outside, the Inner Tracking

System (ITS). The ITS is used to localize the primary vertex, reconstruct the secondary vertices, track and identify particles with low momentum (< 100 MeV) and improve momentum and angle resolution of particles which traverse the TPC [12].

The Time Projection Chamber (TPC) is the main tracking device of ALICE and is used for momentum measurements, particle identification via energy deposition through ionization and vertex determination. Next comes the Transition Radiation Detector (TRD), which is designed to supplement electron identification for momenta above 1 GeV/c [13]. The TRD is surrounded by the Time-Of-Flight Detector (TOF). TOF provides particle identification in the momentum region of 0.2 to 2.5 GeV/c via measurement of the velocity and mass of a particle. The High-Momentum Particle Identification Detector (HMPID) is a ring Cherenkov detector which is dedicated to measurements of identified hadrons for p_T > 1 GeV/c [14]. Two electromagnetic calorimeters, the PHOton Spectrometer (PHOS) and the ElectroMagnetic CALorimeter (EMCal) are the outermost detectors. The ElectroMagnetic CALorimeter provides additional electron identification and efficient triggers for jets, photons and electrons. HMPID, PHOS and EMCal do not cover the full azimuthal and the whole pseudorapidity range of the central barrel.

Additional detectors are located at large rapidities to complement the central detection system to characterize the events and to provide the interaction trigger [15].

The global reference frame used throughout the thesis is as follows: the z axis is parallel to the beam and pointing to the opposite direction of the muon arm, x and y in the transverse plane to the beam direction.

In the following sections the subdetectors used for the analysis presented in this thesis are discussed in more detail. A detailed description of the ALICE experiment and its overall performance can be found in [10] and [12].

2.1 Inner Tracking System (ITS)

The ITS consists of six layers of silicon detectors located at radii r = 4, 7, 16, 24, 39 and 44 cm [10]. Because of the high density of tracks near the collision point the first two strips of layers are Silicon Pixel Detectors (SPD) followed by two layers of Silicon Drift Detectors (SDD). Due to lower multiplicity in the outer layers the two last layers consist of Silicon Strip Detectors (SSD) [14].

The main task of the ITS is to localize the primary vertices with a resolution of 100 μm in the z direction and 12 μm in the x-y plane, reconstruct the secondary vertices from decays of heavy flavour hadrons and also provide tracking and particle identification for momenta below 1 GeV/c [14].
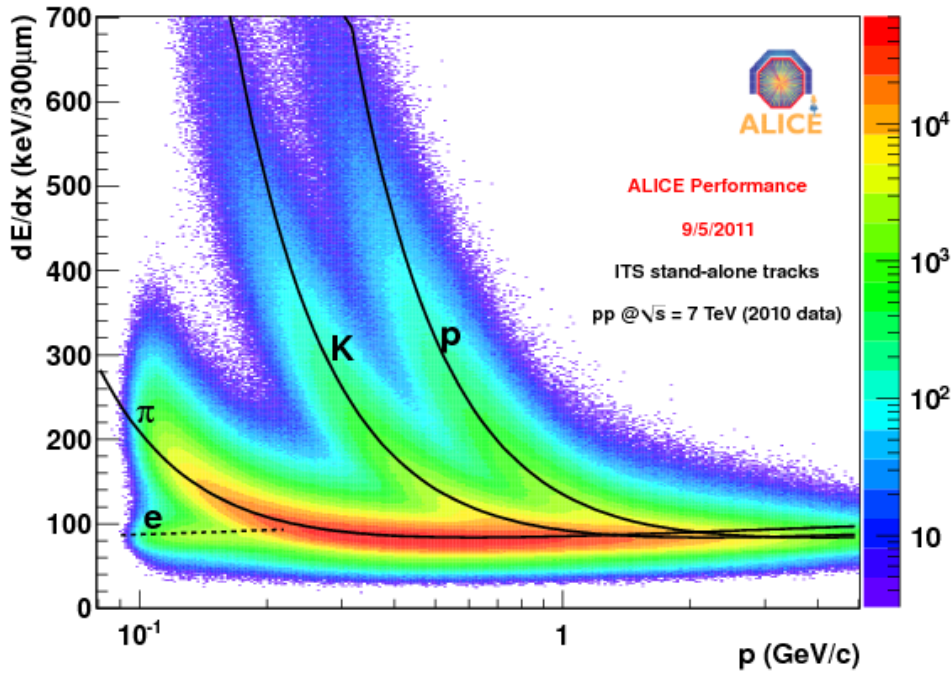

Figure 2.2: dE/dx distribution as a function of the particle momentum measured by the ITS. Picture taken from [16].

Fig. 2.2 shows the measured energy loss dE/dx in the ITS as function of the particle momentum. It provides sufficient separation power between different particle species in the low momentum region of around (< 1 GeV/c). The energy loss due to ionization is measured by the two layers of SDD's and SSD's and calculated with a truncated mean [12].

In this thesis the particle identification capabilities of the ITS are used to improve the separation between hadrons and electrons in the low momentum region (lower 1.5 GeV/c) for the analysis of the Pb-Pb data described in section 3 and section 4.
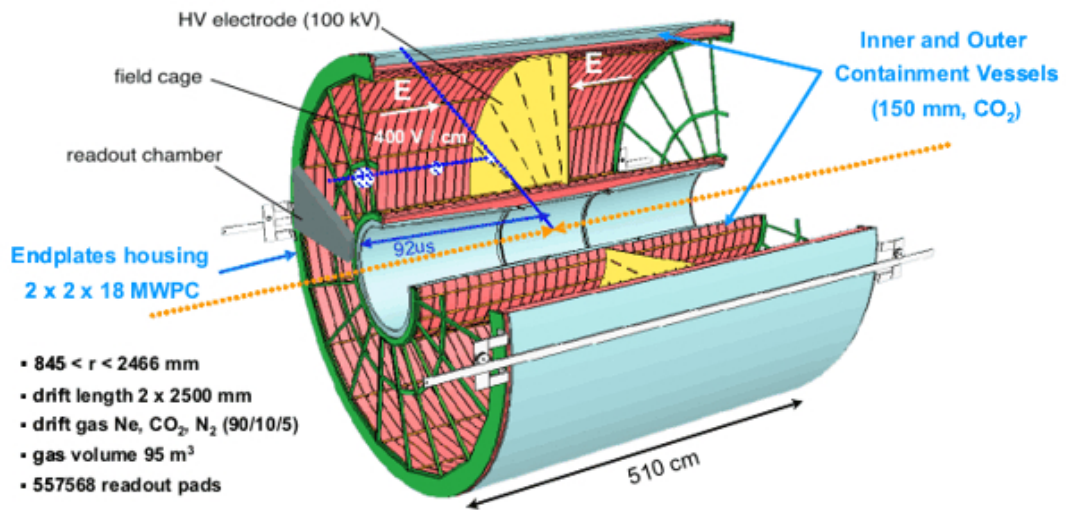
2.2 Time-Projection Chamber (TPC)

Figure 2.3: Schematic layout of the TPC. The picutre is taken from [15].

The TPC is the main tracking detector of the ALICE central barrel and provides good charged particle identification via the energy loss of particles due to ionization. TPC´s layout is shown in Fig. 2.3. The TPC has a cylindrical shape with an inner radius of about 85 cm and a outer radius of around 250 cm with a total length of approximately 500 cm. The cylindric field cage with a volume of 88 m^3 was filled with a mixture of Ne/CO_2 [90:10] in the years 2011-2013 and with a mixture of Ar/CO_2 [88:12] in the years 2015-2016. The central cathode divides the field cage into two parts and creates together with two opposite axial potential dividers a highly uniform electrostatic field with a strength of 400 V/cm parallel to the beam axis. Primary electrons created by ionization of traversing particles drift to the end plates of one of the two sides where multi-wire proportional chambers are installed for readout. Electrons will reach the anode wire, get amplified and induce a signal on the pads. Gating wire grids are installed in front of the readout chambers to prevent ions created in the avalanche process to drift back into the drift volume. In such case, they would create field distorions in the drift field [17].

Particle identification with the TPC is obtained by measuring the energy loss (dE/dx) and the momenta of particles traversing the detector. Fig 2.4 shows the specific energy loss of different particles as function of the momentum. The parametriza-
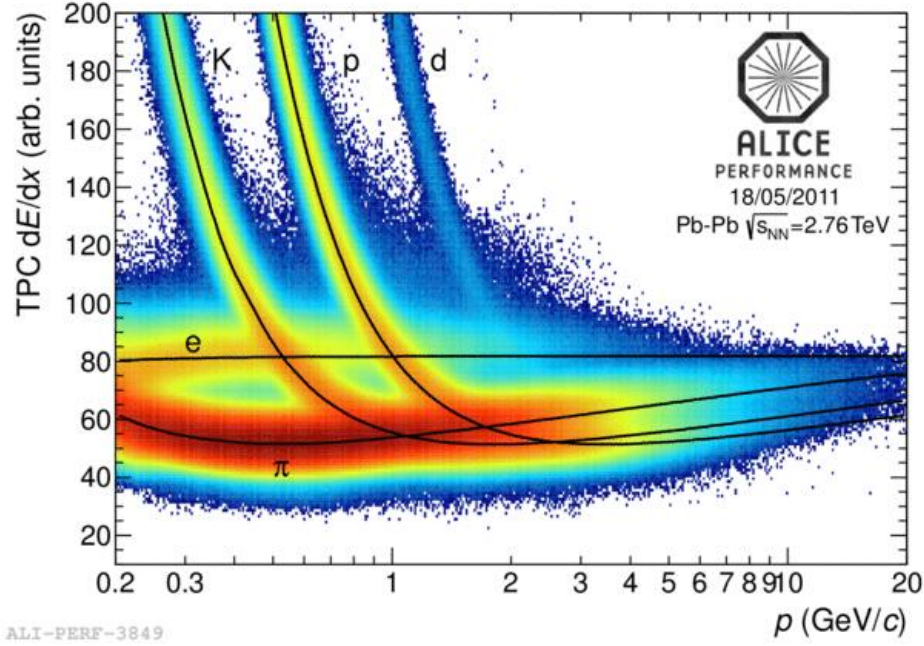
Figure 2.4: Specific ionization loss for different particle species as function of the momentum. The black lines correspond to the parametrization describing different particle species[15]

tion of the detector response is based on the Bethe- Bloch formula, which according to [14] for the ALICE TPC is

$$\frac{dE}{dx} = \frac{C_1}{\beta^2}(ln(C_2\beta^2\gamma^2) - \beta^2 + C_3) \tag{2.1}$$

with $\gamma = \sqrt{1-\beta^2}$, $\beta = v/c$ and C_1, C_2 and C_3 being detector-specific constants.

2.3 Time-Of-Flight detector (TOF)

The Time-Of-Flight detector provides particle identification via measuring the time of flight t of a particle. It has a cylindrical shape with an inner radius of 370 cm, an outer radius of 390 cm and an overall longitudinal length of 745 cm. The basic unit of the TOF system is a 10-gap double-stack Multi- Gap - Resistive chambers (MRPC) strip, 122 cm long and 13 cm wide [10].

Fig. 2.5 shows the concept of the MRPC. A high voltage is applied at the opposite surface of the stack, which is filled with a gas. When a charged particle traverses the stacks, it will ionize the gas and the high voltage will amplify the signal, creating an

electron avalanche, which is detected by the plates. Summing up the signals of each gap results in the total signal.
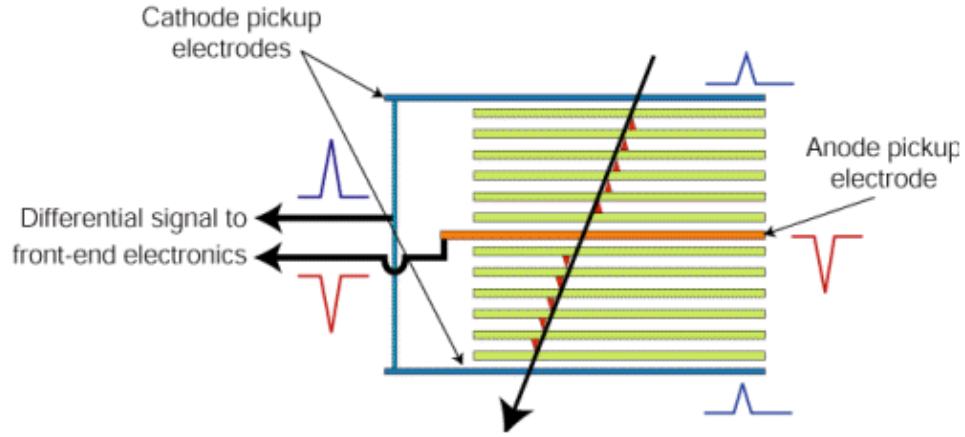

Figure 2.5: Principle of the Multi-Gap-Resistive chambers used in the ALICE-TOF. The black arrow shows a track which traverses the TOF. Picture taken from [18]

A Time-Of-Flight detector measures the time-of flight t and the distance L of the trajectory. Combined with the momentum of the particle, measured from the bended trajectory of the particles due to a magnetic field, the following equation for the particles mass can be aquired [19]:

$$m = \frac{p}{c}\sqrt{\left(\frac{ct}{L}\right)^2 - 1} \qquad (2.2)$$

The difference of time of flight between two particles A and B with the same momentum can be obtained through the equation [19]:

$$|t_A - t_B| = \frac{L}{c}\left|\sqrt{1 + \left(\frac{m_A c}{p}\right)^2} - \sqrt{1 + \left(\frac{m_B c}{p}\right)^2}\right| \qquad (2.3)$$

In the relativistic limit ($p \gg mc$) we can use the following approximation, obtained

from the Taylor expansion:

$$\sqrt{1 + \left(\frac{mc}{p}\right)^2} \approx 1 + \left(\frac{(mc)^2}{2p^2}\right) \tag{2.4}$$

Therefore the separation power of two particles is given by

$$n_{\sigma_{TOF}} = \frac{|t_A - t_B|}{\sigma_{TOF}} = \frac{Lc}{2p^2\sigma_{TOF}}|m_A^2 - m_B^2| \tag{2.5}$$

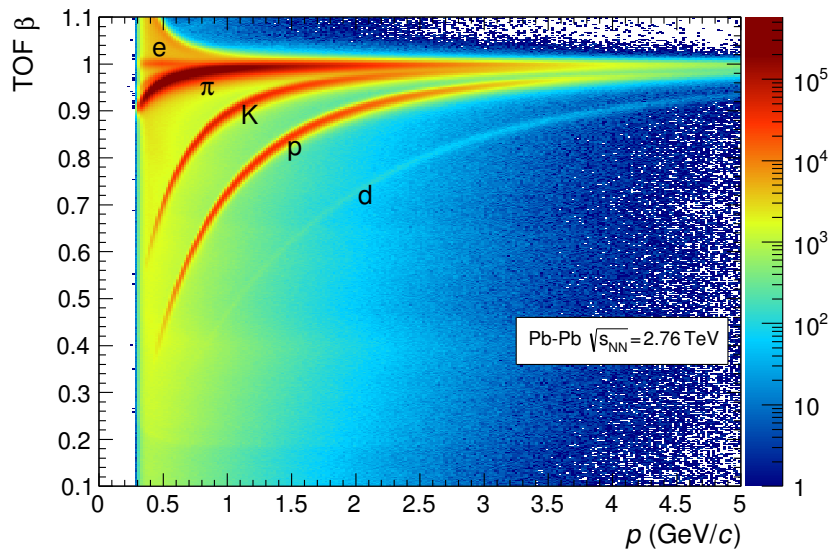Figure 2.6: Distribution of β as measured by the TOF detector as a function of momentum for particles reaching the TOF in Pb-Pb interactions [12].

Fig 2.6 shows the distribution of β as function of the particles momentum, using the information from the TOF detector. TOF provides good particle identification up to momenta up to 2.5 GeV/c for pions and kaons and up to 4 GeV/c for pions and protons [12].

2.4 Transition Radiation Detector (TRD)

The TRD is designed to provide electron identification at momenta above 1 GeV/c and consists of 540 individual readout detector modules which are arranged into 18 super modules [10]. Only 10 out of 18 super modules were installed in the year 2011, whereas all 18 were used for the data taken in 2015.

Particle identification with the TRD is based on the energy loss via ionization in a gas and transition radiation of electrons which will provide good separation capabilities between electrons and pions.

Transition radiation is produced when ultra relativistic charged particles ($\gamma > 10^3$) traverse the boundary between two materials with different dielectric constants [12]. In our momentum region of interest (1-100 GeV/c) only electrons can create transition radiation due to their little mass.
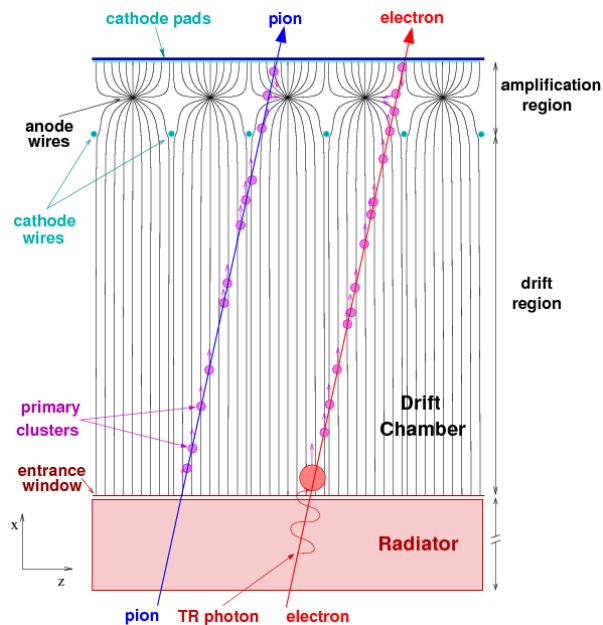
Figure 2.7: Showing a layer of the TRD. One can clearly see the radiator, drift chamber and the amplification zone. Picture taken from [21].

Fig 2.7 shows a layer of a TRD module, each of them are composed of a radiator, a drift chamber and the front end electronics. The particle traverses through the radiator into the drift chamber. This drift chamber is filled with a gas mixture of Xe-CO_2 [85:15] [12]. The traversing particle creates primary electrons by ionizing the gas, which move to the amplification region and are then able to be measured by the

Figure 2.8: Average pulse height of the TRD signal for pions and electrons in dependency of the drift time the primary electrons in the cluster need to reach the readout electronics. Picture taken from [20].
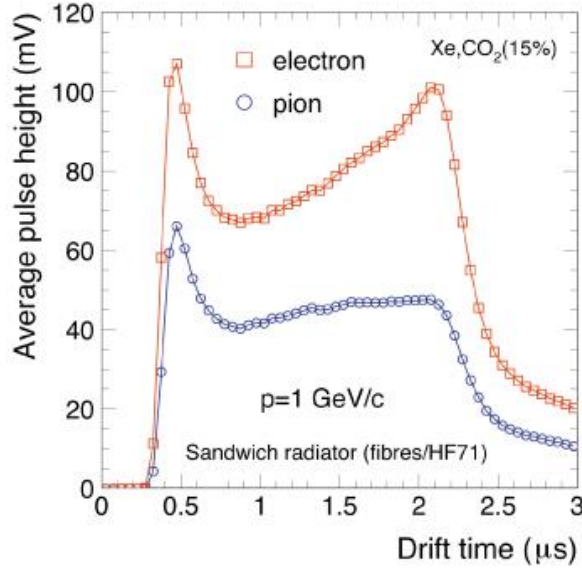
front end electronics, where multi wire proportional chambers are mounted.

The average pulse height as function of the drift time for pions and electrons is shown in Fig. 2.8. For electrons two peaks are observed. The first peak at early drift times is due to the charge deposit in the amplificiation region, where charges drift from both sides to the anode wire. The peak at late drift times corresponds to the photon created through transition radiation and absorbed by the gas near the radiator [13]. For pions only one peak is observed since they are not able to create transition radiation at the momentum region of interest.

One method for particle identification with the TRD is the bidimensional likelihood method (LQ2D). The likelihood to be an electron is according to [7]:

$$L = \frac{P_e}{P_e + P_\pi}; \ P_e = \prod_{i=1}^{n} P(X_i|e); \ P_\pi = \prod_{i=1}^{n} P(X_i|\pi) \quad (2.6)$$

where N is the number of detector layers and $P(X_i|e)$, $P(X_i|\pi)$ are the probabilities that a detector signal in layer i was produced by an electron/pion [7].

The bidimensional likelihood method uses the fact that the charge deposit in the TRD has a dependence on the drift time. The TRD signal shown in Fig. 2.8 is divided into two halves for each layer. For each layer and half, the probability that the signal in one half belongs to a electron or pion is determined in a way similar to the one for the one dimensional likelihood described in eq. (2.6).

2.5 Electromagnetic Calorimeter (EMCal)

The EMCal is a large Pb- scintillator sampling calorimeter with cylindrical geometry, located adjacent to the ALICE magnet coil at a radius of $\sim$ 4.5 meters from the beam line. It covers the pseudorapidty of $-0.7 < \eta < 0.7$ and an azimuthal angle of $\Delta\Phi = 107°$. The relative position of the EMCal is shown in Fig. 2.9.
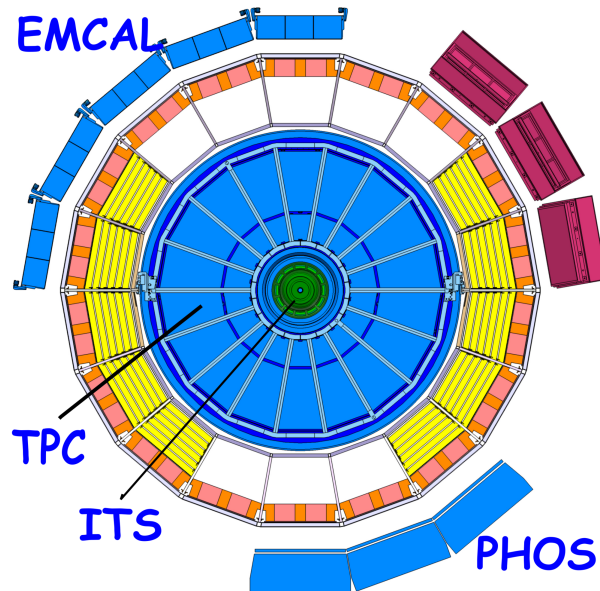
Figure 2.9: A section of the ALICE detector in the year 2011. Picture taken from [24]

Particles produce an electromagnetic shower when traversing the detector. Due to the choice of the cell size and the detector thickness of around 20.1 radiation lengths, the shower produced by a particle is used to discriminate between electromagnetic and hadronic particles. Electrons and photons will deposit their total energy in the detector, while hadrons will only deposit a fraction of their energy. The EMCal will provide good electron identification capabilites in the traverse momenta region of

above 3 GeV/c [22].

In this analysis the ratio E/p of the energy deposit in the EMCal E and the momentum of the corresponding track p is used. An EMCal cluster is called "matched" to a reconstructed track when the distance of the track and the cluster have a certain, changeable value [23].

Additionally to the electron identification abilities the EMCal detector provides fast and efficient triggers for jets, photons and electrons, which will be explained in more detail in section 5.4.

2.6 PID signal in ALICE

The response of each detector can be expressed in terms of its raw signal S. The signal S corresponds for the TPC and ITS to the specific energy loss dE/dx and for TOF to the expected time-of-flight t_{TOF}. One possible approach is to define a discriminating variable ξ, which makes use of the expected detector response R:

$$\xi = f(S, R), \tag{2.7}$$

where R can depend on the properties of the particle track, like the momentum p or the track length L [25].

For a Gaussian response, for example the dE/dx response of the TPC after subtraction of the Landau tail by using a truncated mean, the response function R can be described by the expected average signal $\hat{S}(H_i)$, where H_i describes the particle species and σ the expected signal resolution.
The most commonly used discriminating variable for PID is the n_σ variable defined as the deviation of the measured signal from that expected for a species H_i in terms of the detector resolution:

$$n_{\sigma_\alpha^i} = \frac{S_\alpha - \hat{S}(H_i)_\alpha}{\sigma_\alpha^i}, \tag{2.8}$$

where α = (ITS,TPC,TOF) [25].

Therefore, a particle track now corresponds to a given particle species if the value

$n\sigma_\alpha$ lies within a certain range around the expectation. For example a cut in the TPC around $-2 < \sigma_{TPC}^e < 2$ means that tracks with a σ_{TPC}^e around [-2,2] are identified as electrons.

The detector signal of ITS, TPC and TOF will be described throughout the thesis in values of $n\sigma_\alpha^i$.

3 Estimating the electron purity in Pb-Pb at $\sqrt{s_{NN}} = 2.76$ with different fitting methods

For the analysis of heavy flavour hadron decay electrons its important to know how strong electron candidates are contaminated by other particles. In a first step electron candidates are identified with the ITS, TPC and TOF detector. The remaining hadron contamination of the electron candidates is then derived via fits in the TPC dE/dx distributions. These hadrons are then subtracted from the spectrum of the electron candidates. The electron spectrum obtained through this procedure does not only contain electrons from heavy flavour hadron decays, but also electrons from their decay channels like the darlitz decay or photon conversions.

One approach to subtract the electrons from other decay channels is the cocktail method in which the background electrons are calculated from measured spectra of these decay sources using Monte-Carlo generators. It's therefore crucial for heavy flavour hadron decay electron analyses to know how many of the electron candidates mentioned above are actual electrons.

This is why the electron purity and the hadron contamination of electron candidates, obtained in Pb-Pb collisions recorded in the year 2011, are estimated with two different fit methods in this part of the thesis. The first fit method uses templates extracted from data to estimate the hadronic contamination in the TPC dE/dx for different momentum slices, whereas the second method parametrizes the hadron contamination with different functions. Both electron purity and hadron contamination obtained with both fit methods are compared and discussed in the following.

3.1 Data Set and track selection

In this part of the thesis lead-lead collisions recorded in 2011 at $\sqrt{s_{NN}}$ = 2.76 TeV are analysed. This analysis concentrates on most central events of the 0 - 10% centrality where a total number of 1.4e+07 events are recorded. The track and event selection criteria which each track has to satisfy are described in the following.

A minimum of 110 - out of 159 - produced clusters in the TPC are required, from which at least 90 clusters are used for particle identification. Additionally, a signal for each track in at least five layers of the ITS is required in order to make use of its PID capabilities. Moreover, we demand to have a signal in both layers of the SPD for every track. This will guarantee that electrons originate in processes near the vertex and not from pair production of photons at an outer radius.

A summary of all applied track selection criteria is shown in table 3.1.

description	cut value
No. of TPC clusters	≥ 110
No. TPC clusters used in PID	≥ 90
Minimum Ratio for TPC clusters	≥ 0.6
χ^2 per TPC cluster	≤ 3.5
No. of layer signals in ITS	≥ 5
Hit in first two layers	kBoth
χ^2 per ITS cluster	≤ 36
Check ITS Layer Status	kFALSE
Vertex Range in z- direction	$< |10|$
No. of TRD Tracklets	≥ 0
pseudorapitdy $|\eta|$	< 0.8

Table 3.1: Track selection criteria used in this analysis.

3.2 Selection of the electron candidates

After the track selection criteria, summarized in table 3.1, are applied to each track, electron candidates are identified by selecting in TOF around the electron expectation value $-2 < \sigma_{TOF}^e < 2$ and in the ITS around $-1 < \sigma_{ITS}^e < 1$ for p < 1.5 GeV/c and $-2 < \sigma_{ITS}^e < 2$ for p $\geq$ 1.5 GeV/c. The selection criteria in the ITS is loosened for higher momenta (p $\geq$ 1.5 GeV/c), because ITS PID is not helping to reduce the hadronic background any further.
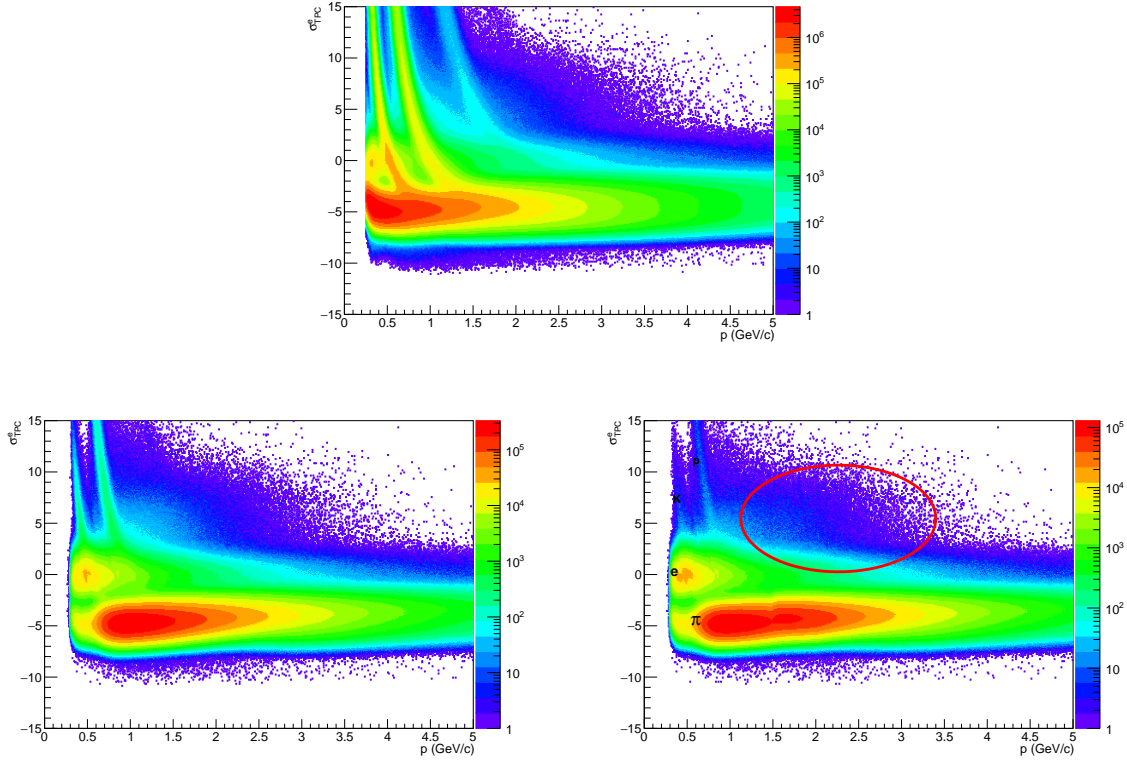
Figure 3.1: nσ_{TPC}^e distribution as function of the momentum p for the Pb-Pb data recorded in 2011 before PID (top panel), after TOF PID (bottom left panel) and after TOF and ITS PID (bottom right panel). The bottom right panel shows the electron candidates which are analysed further.

Fig. 3.1 shows the sample of tracks satisfying the track selection criteria in table 3.1 after different steps in the PID selection. Since the signal of the TPC is given in nσ_{TPC}^e (see section 2.6) electrons are located in the region of $\sigma_{TPC}^e \approx 0$. The nσ_{TPC}^e distribution is seen in the top panel of Fig. 3.1 before applying TOF and ITS PID, whereas the bottom left panel of Fig. 3.1 shows the tracks identified after applying the TOF selection criteria mentioned above. After TOF PID the deuteron band vanishes, while protons and kaons are still visible, contaminating the nσ_{TPC}^e distribution. Additionally, after TOF and ITS PID a cloud (red ellipse in the bottom right panel) which cannot be removed with the used PID selection criteria still remains. The composition of this cloud and the effect of contamination on the electron candidates are discussed in the following section.

3.3 Template method

After selecting our electron candidates there still remain a hadron contamination in the sample. To estimate this remaining hadron contamination, the sample shown in the bottom right panel of Fig. 3.1 is divided into several momentum slices and projected onto the $n\sigma_{TPC}^e$.

An example of this projection is shown in Fig. 3.2 for the momentum 0.8 GeV/c to 0.9 GeV/c. Two peaks are observed, where the peak at around $n\sigma_{TPC}^e = 0$ corresponds to electrons since we are plotting the TPC dE/dx signal in values of $n\sigma_{TPC}^e$. The peak emerging on the left side of the electrons at negative $n\sigma_{TPC}^e$ can be described by pions, expected to have contributions to those projections over the entire momentum range analysed in this section. The tail on the right hand side at positive $n\sigma_{TPC}^e$ describes the cloud seen in the $n\sigma_{TPC}^e$ distribution of the electron candidates.
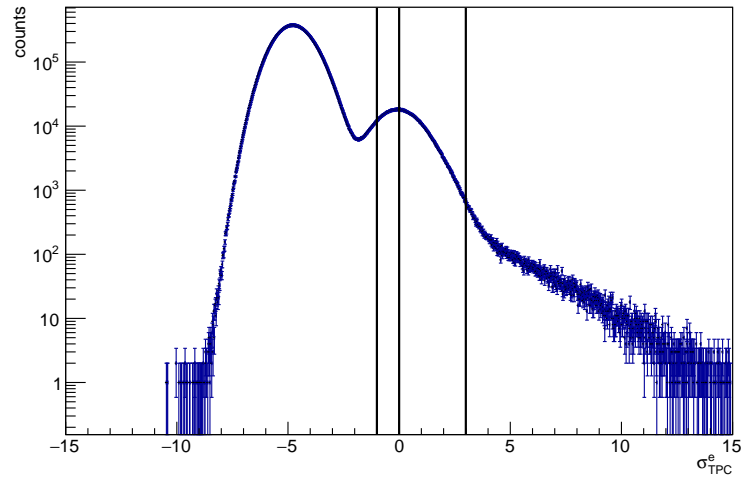

Figure 3.2: Projection of the $n\sigma_{TPC}^e$ for the momentum from 0.8 GeV/c to 0.9 GeV/c. The black lines show the $n\sigma_{TPC}^e$ interval -1 to 3 and 0 to 3 in which the hadron contamination of our electron candidates is evaluated.

The idea behind the template method is now to identify the different particle species, in our case protons, kaons and pions, by applying different selection criteria with TOF and the TRD to the data set. The $n\sigma_{TPC}^e$ signal as function of the momentum for the different particle species is then divided into several momentum bins with the same binning as for the electron candidates and projected on the $n\sigma_{TPC}^e$. This projections of the $n\sigma_{TPC}^e$ signal are called templates and are used to describe the

hadronic contamination due to protons, kaons and pions to our electron candidates, shown in Fig. 3.2.

Fig. 3.3 shows the nσ^e_{TPC} distribution as function of the momentum for protons, pions, kaons and deuterons, after the selection criteria explained in the following:

The nσ^e_{TPC} distribution for protons shown in the top left panel of Fig. 3.3 is obtained by applying track selection criteria in TOF around the proton expectation value of $-2 < \sigma^p_{TOF} < 2$. Protons are identified by the red band in the distribution, but there still remain misidentified pions, electrons and kaons which cannot be removed by the TOF detector (see Fig. 2.6). In order to keep the relative contamination of the protons due to other particles low, a template for protons is only used in the momentum regions where the red proton band crosses the electron band, which is the case at around 1 GeV/c. But even in this region, where the protons dominate the nσ^e_{TPC} distribution, the relative contamination due to electrons, pions and kaons cannot be excluded completely. This of course will lead to a underestimation of the electron purity, which is discussed later.

As described in section 2.3, TOF alone does not have the capabilities to distinguish between electrons and pions due to the small mass difference. Therefore, in addition to a TOF selection in $-2 < \sigma^\pi_{TOF} < 2$, the information from the TRD is used to reject electrons from the nσ^e_{TPC} distribution. The pion nσ^e_{TPC} distribution is shown in the top right panel of Fig. 3.3. As explained in section 2.4 the method of particle identification with the TRD used in this analysis is the bi-dimensional likelihhood (LQ2D). A track is identified as a pion, when the electron probability is below 10%. As we can see, there still remains a contamination of kaons and protons in the nσ^e_{TPC} distribution of pions, seen by the two corresponding bands, since the TRD is only rejecting electrons. A contamination of the nσ^e_{TPC} distribution due to electrons especially in the low momentum (below 1 GeV/c) is expected as well since the electron rejection of the TRD below 1 GeV/c is not as good as for the high momentum region. In the sample remains a big cloud, which cannot be removed by either TOF or TRD.

Also for the kaon nσ^e_{TPC} distribution the TRD is used in addition to the TOF selection of $-2 < \sigma^K_{TOF} < 2$. If the electron and the pion probability is below 10%, a track is identified as a kaon. The kaon nσ^e_{TPC} distribution is shown in the bottom
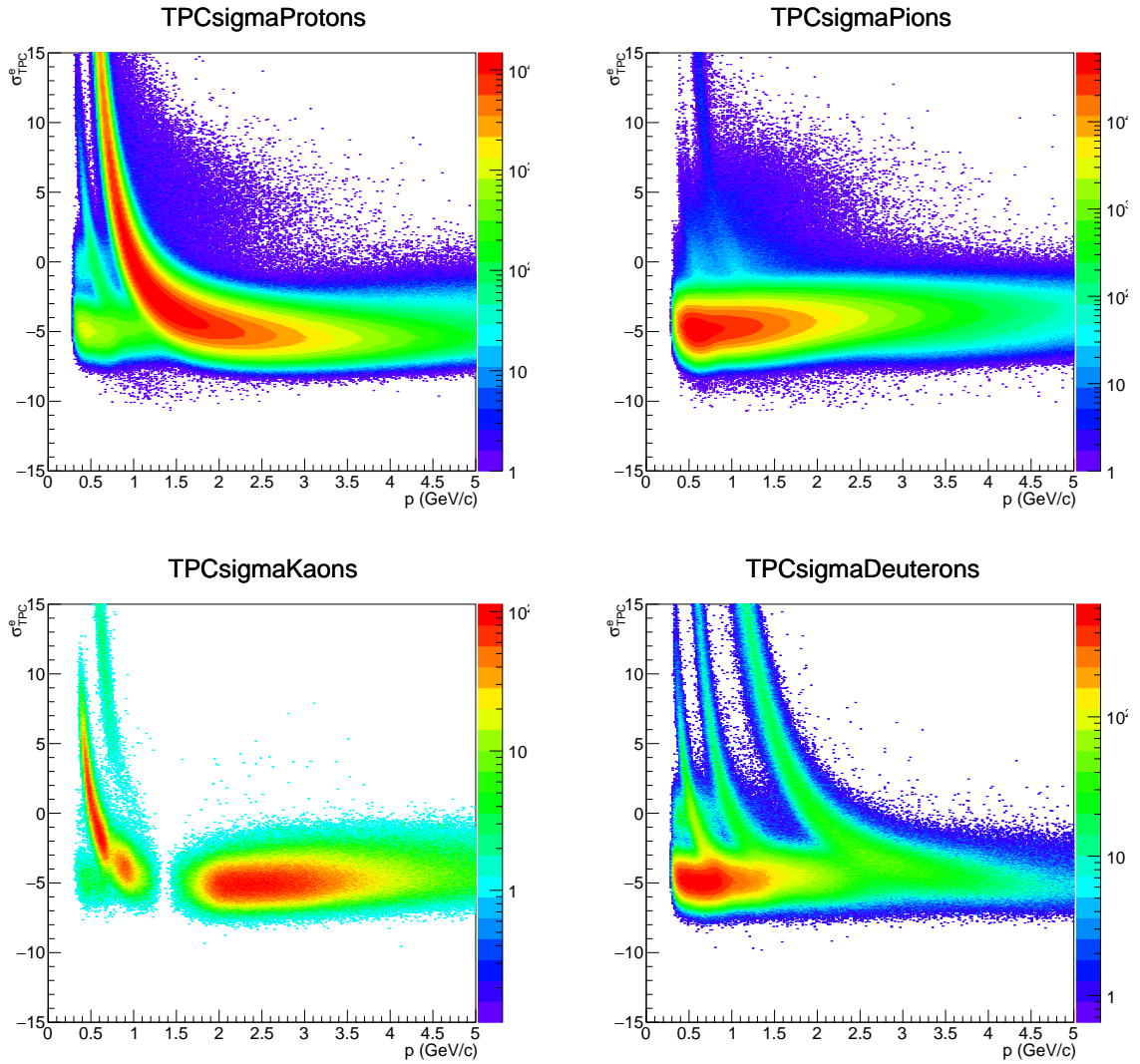
Figure 3.3: nσ_{TPC}^e distribution as function of the momentum for protons (top left panel), pions (top right panel), kaons (bottom left panel) and deuterons (bottom right panel), for the Pb-Pb data set recorded in 2011, obtained with the PID selection described in section 3.3.

left panel of Fig. 3.3. It´s observed that protons are separated distinctly from kaons. The contamination of kaons due to electrons is also under control since a template for kaons is only extracted from the distribution at momentum of around 0.5 GeV/c where the kaon band crosses the electron band. For higher momenta (above 1.5 GeV/c) we can observe many particles in the negative $n\sigma^e_{TPC}$. These are kaons and pions which already crossed the electron band and cannot distinguished very well by TOF and TRD at high momenta.

For completeness the $n\sigma^e_{TPC}$ distribution for deuterons, obtained within the $n\sigma^d_{TOF}$ interval from -2 to 2, is shown in the bottom right panel of Fig. 3.3. Nevertheless, a template for deuterons is not used in this analysis since the deuteron band is removed entirely in the $n\sigma^e_{TPC}$ distribution of the electron candidates after TOF and ITS PID as shown in Fig. 3.1. We can also observe that the $n\sigma^e_{TPC}$ distribution for deuterons contain the Bethe - Bloch bands of several particle species, while the deuteron band is not even dominating the distribution. This would lead to unclean templates. Therefore, the contribution of deuterons to the hadron contamination of the electron candidates can be neglected.
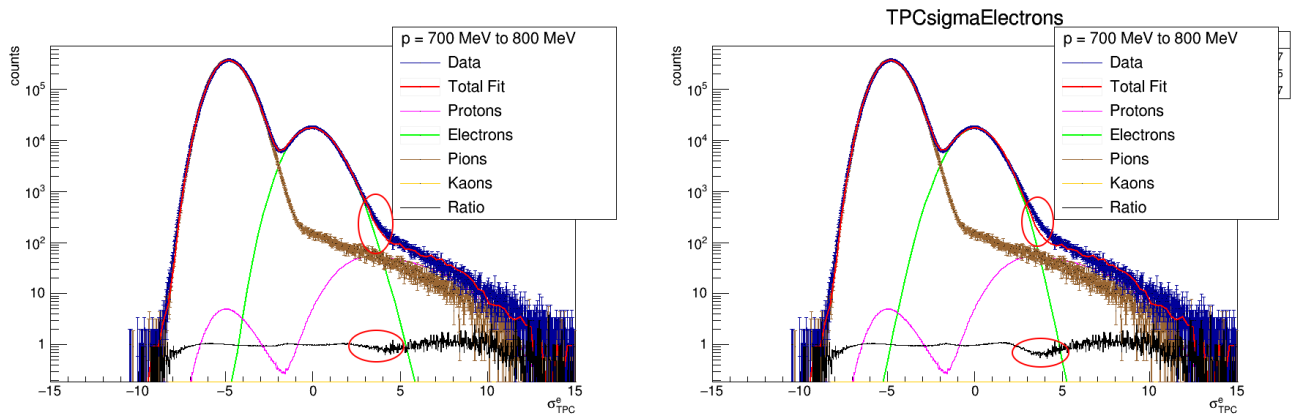

Figure 3.4: $n\sigma^e_{TPC}$ distribution for the momentum 0.75 ± 0.05 GeV/c with electrons described by a convolution of Landau and exponential function (left panel) and by a Gaussian distribution (right panel).

For the parametrization of electrons in the momentum slices of the $n\sigma^e_{TPC}$ two different functions have been tested: a convolution of a Landau function with a exponential function $exp(\alpha \cdot x)$ and a Gaussian distribution. Fig. 3.4 shows the p slice in $n\sigma^e_{TPC}$ for the momentum p = 0.75 ± 0.05 GeV/c with the electrons parametrized

by a convolution of Landau and exponential function (left panel) and a Gaussian distribution (right panel). The black line in both fits describes the ratio of data (blue markers) and fit (red line). In the right panel at around $n\sigma^e_{TPC} \approx 4$ (marked with the red circles) we can observe that the Gaussian distribution does not explain the shoulder on the right side of the electrons, which is also marked as red circle, as well as the convolution shown in the left panel. The same conclusion can be made by looking at the reduced χ^2 for both electron parametrizations. For the Gaussian distribution χ^2_{red} = 45.2 was calculated for the reduced χ^2, whereas χ^2 = 42.1 was calculated for the convolution. This observation is also made for the other p slices in $n\sigma^e_{TPC}$, analysed in this chapter of the thesis. We can therefore conclude that the convolution of Landau and exponential function are overall superior in describing the data set than the Gaussian distribution.

It´s now possible to obtain the templates for each particle species by projecting the $n\sigma^e_{TPC}$ distribution shown in Fig. 3.3 onto the $n\sigma^e_{TPC}$ for different momentum slices. Those templates are fitted to the p slices of the electron candidates. The following fit function is applied:

$$f(x) = A_e \cdot L(\mu_e, \sigma_e, x) \cdot exp(\alpha_e x) + S_p \cdot T_p(x) + S_K \cdot T_K(x) + S_\pi \cdot T_\pi(x) \qquad (3.1)$$

with x describing the energy loss dE/dx in the TPC described in $n\sigma^e_{TPC}$, L the Landau distribution , T_i the templates for the different particle species and S_i a scaling factor to scale the templates to the data, with i = (p,K,π). The fit parameter are described by μ_e, σ_e and S_i.

Fig. 3.5 shows the fits done with the templates for different p slices in the low, mid and high momentum region. As mentioned above, a template for protons is only used in the momentum region of 1 GeV/c and a template for kaons only in the region of 0.5 GeV/c. For momenta above 1.5 GeV/c only the pion template is used to describe the total hadron contribution in the p slices in $n\sigma^e_{TPC}$ since protons and kaons start to overlap with the pion band after crossing the electron line in negative $n\sigma^e_{TPC}$ in the high momentum region. This is visible by looking at the two bottom panels of Fig. 3.5 where a second peak starts to emerge on the left side of the pion peak at around $\sigma^e_{TPC} \approx -6$.

Moreover, looking at Fig. 3.5 we can now explain the content of the cloud mentioned
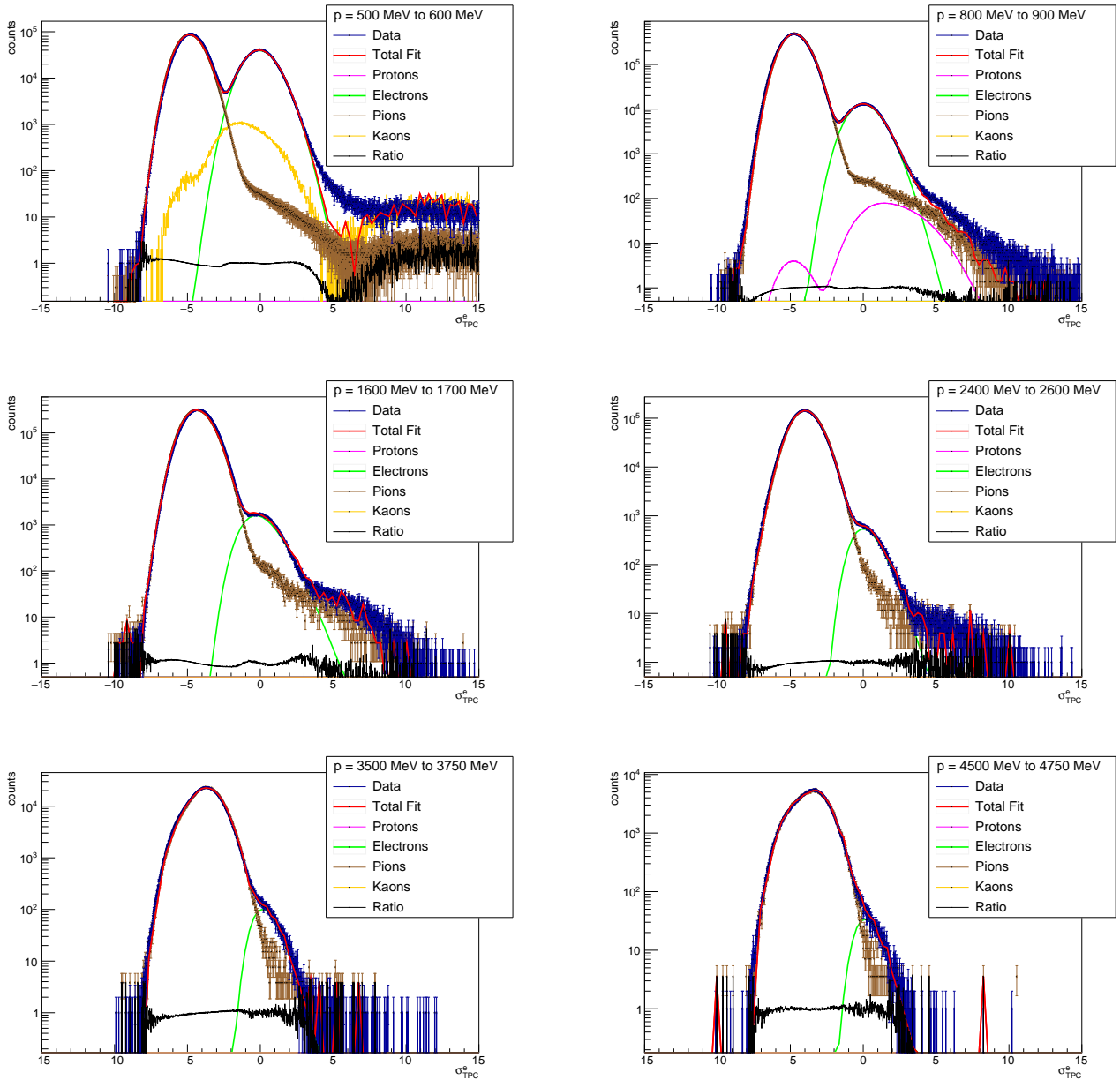
Figure 3.5: Distribution of the $n\sigma_{TPC}^{e}$ in six different momentum ranges. The distributions are fitted with the fit function in equation (3.1). For high momenta only the pion template is used to explain the hadron contamination.

in section 3.2 by fitting with templates. The cloud corresponds in the momentum slices in $n\sigma^e_{TPC}$ to the tail on the right side of the electron peak. In Fig. 3.5 we can see that the tail on the right side of the electron peak can be described by the pion template and can therefore conclude that the main contriubtion to the cloud are primarily pions.

Nevertheless, its clearly visible that the pion template cannot fully describe the tail on the right side of the electron peak. The pion tail is underestimated by the pion template, which can be observed in the low and mid momentum region (see top four panels of Fig. 3.5). This may have the following reason.

In Pb-Pb collisions, since a high particle multiplicity is expected, particle tracks exist which traverse the TPC close to each other and therefore cannot be separated very well. If these tracks also had overlapping clusters in the TRD, it would lead to a higher energy loss in the TRD than expected for pions. The in section 2.4 described bi-dimensional likelihood (LQ2D) that a track is assigned to a electron would be higher than the bi-dimensional likelihood that the track is assigned to a pion. This on the other hand means that the overlapping tracks are identified as electrons and are rejected from the pion template which leads to an underestimation of the tail on the right side of the electrons in the momentum slices in $n\sigma^e_{TPC}$. The underestimate tail is observed up to a momenta of 3 GeV/c, as shown in the top four panels of Fig. 3.5.

Describing the hadrons in the momentum slices with templates has given us an insight of what particles contribute to the cloud seen in the $n\sigma^e_{TPC}$ distribution of the electron candidates. Since those templates are also contaminated with other particles because they are extracted directly from the data it will lead to a decrease of the electron purity.

In order to prevent this, a second fit method is presented to describe the hadron contamination of our electron candidates.

3.4 Standard fit method

In the following section a second fit method is described, which is based on the parametrization of the particles by different distributions. Since this is the usually used method to estimate the hadron contamination of electron candidates in many heavy flavour hadron decay electron analyses, it is called the standard fit method.

In this approach electrons are described by a convolution of a Landau distribution with an exponential function $exp(\alpha \cdot x)$ like it was done in section 3.3. The same parametrization is now also used for pions emerging left to the electron peak. To describe the pion tail on the right side of the electron peak an additional Gaussian distribution is used. For higher momenta a second Gaussian is introduced to explain the hadrons that have already crossed the electron band and start emerging beside the pions at negative $n\sigma^e_{TPC}$.

Like for the template method the fit routine can now be applied for different momentum slices in $n\sigma^e_{TPC}$ with the following fit function:

$$f(x) = A_e \cdot L(\mu_e, \sigma_e, x) \cdot exp(\alpha_e x) + A_\pi \cdot L(\mu_\pi, \sigma_\pi, x) \cdot exp(\alpha_\pi x)$$
$$+ A_p \cdot G(\mu_p, \sigma_p, x) + A_{bg} \cdot G(\mu_{bg}, \sigma_{bg}, x) \tag{3.2}$$

where x stands for the energy loss dE/dx in the TPC described in $n\sigma^e_{TPC}$, the first term describes the electrons, the second term the pions, the third term the protons and kaons which already crossed the electron band and start emerging beside the pions in the negative $n\sigma^e_{TPC}$ and the last term corresponds to the background Gaussian. The fit parameters are described by μ_i, σ_i and A_i with i = (e,π,p,bg).

Fig. 3.6 shows the fits done with eq. (3.2) for the same low, mid and high momentum regions as for the fits obtained by the template method. We can observe that the background Gaussian (yellow line) describes the pion tail on the right side of the electrons quite well, but has some problems in the low momentum region up to 1 GeV/c (shown in the top two panels of Fig. 3.6).
Overall it can be observed that the standard fit method describes the data set better than the template fit method. In order to see the contrast of both methods one can compare the ratio (black marker) of data (blue marker) and fit (red line) for fits done with both the template (Fig. 3.5) and the standard fit method (Fig. 3.6). The ratio obtained trough the template method is near the pion tail below unity, whereas the ratio obtained by the standard fit method is at unity. This can be explained by the fact that in the standard fit approach the pion peak and the tail are described by two independent functions (background Gaussian (yellow line) and the pion Landau (brown line)), where for the template method both are explained by the pion template (brown marker).
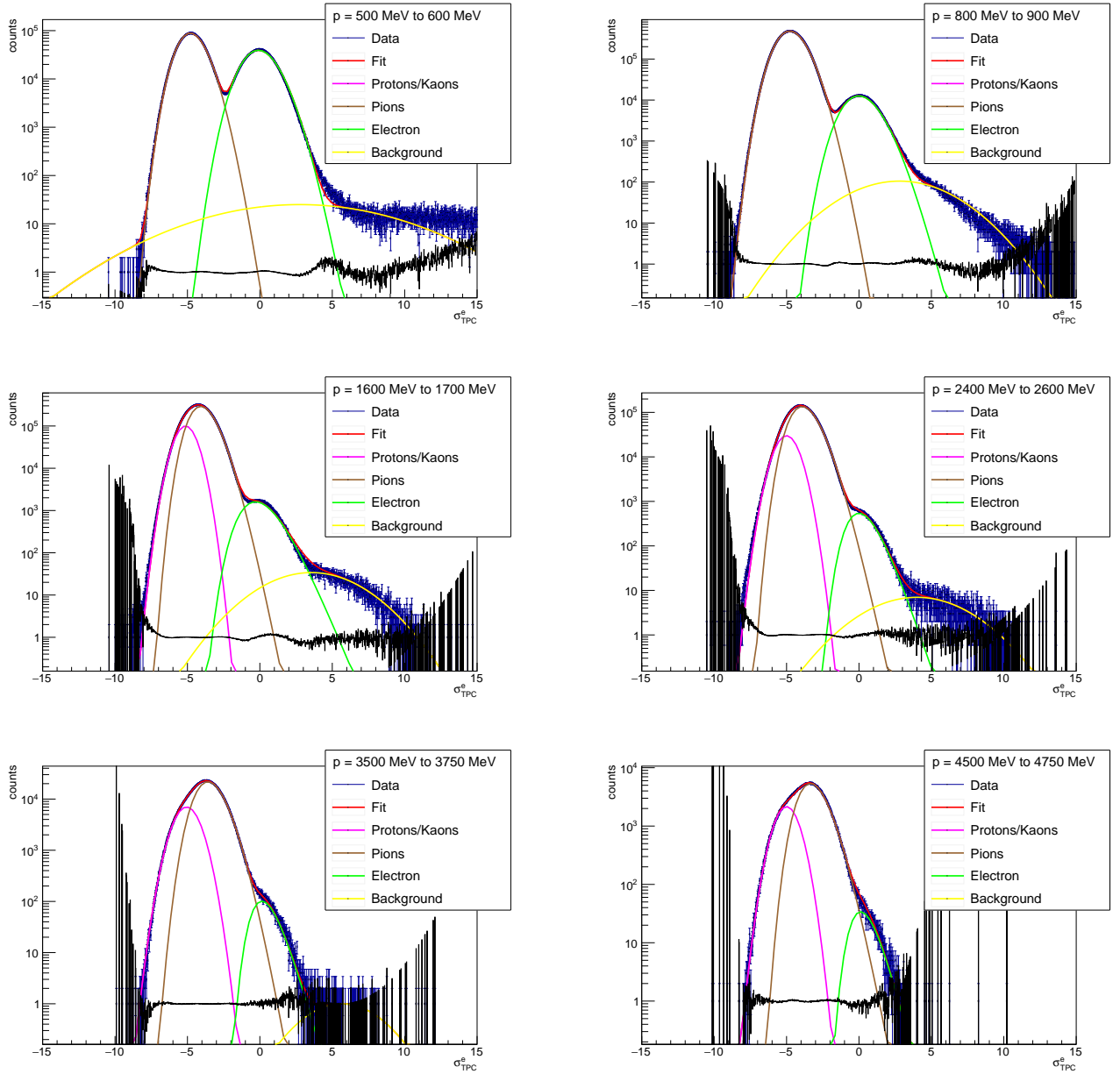
Figure 3.6: Distribution of the $n\sigma^e_{TPC}$ in six different momentum ranges. The distributions are fitted with the fit function in equation (3.2).

3.5 Electron purity and hadron contamination

Both fit routines are now applied for several momentum slices in $n\sigma^e_{TPC}$ in the momentum region from 0 GeV/c to 5 GeV/c. Since the statistics deteriorate for higher momenta the bins are enlarged to obtain better statistics. The binning used in this analysis is the following:

- p = 0 - 2 GeV/c → Δp = 0.1 GeV/c

- p = 2 - 3 GeV/c → Δp = 0.2 GeV/c

- p = 3 - 5 GeV/c → Δp = 0.25 GeV/c

The electron purity and hadron contamination for our electron candidates are obtained via integration of different templates or distributions over the $n\sigma^e_{TPC}$ interval from 0 to 3 and -1 to 3 as shown in Fig. 3.2 as black vertical black lines for the momentum slices above.

The electron purity and the hadron contamination are calculated by following formula:

$$P = \frac{N_e}{N_{Hadrons} + N_e}, \quad C = \frac{N_{Hadrons}}{N_e + N_{Hadrons}} \tag{3.3}$$

$$N_e = \int_u^3 A_e \cdot L(\mu_e, \sigma_e) \cdot exp(\alpha_e x) \, dx, \tag{3.4}$$

$$N_{Hadr.} = \int_u^3 T_K \cdot S_K \, dx + \int_u^3 T_\pi \cdot S_\pi \, dx + \int_u^3 T_p \cdot S_p \, dx \tag{3.5}$$

$$N_{Hadr.} = \int_u^3 A_{bg} \cdot G(\mu_{bg}, \sigma_{bg}, x) \, dx + \int_u^3 A_\pi \cdot L(\mu_{\pi,x}, \sigma_\pi)$$
$$\cdot exp(\alpha_\pi x) \, dx + \int_u^3 A_p \cdot G(\mu_p, \sigma_p, x) \, dx \tag{3.6}$$

where u = -1 or 0, equation (3.5) is used for the template method and equation (3.6) for the standard fit method.

The statistical uncertainty for the particle species are given by:

$$\Delta N_e = \sqrt{N_e}, \quad \Delta N_{Hadr.} = \sqrt{N_{Hadr.}} \tag{3.7}$$

The uncertainties on for the electron purity and hadron contamination are obtained by error propagation.

The electron purity and the hadron contamination received via both fit methods is shown in Fig. 3.7. The top left panel shows the electron purity for the $n\sigma^e_{TPC}$ interval of 0 to 3. Up to p = 0.8 GeV/c the electron purity for both fit models is approximately 98%. Then the electron purity is decreasing to a value of 95% / 88% up to 3 GeV/c for the standard fit routine/template method. For even higher momenta a faster drop in electron purity is observed for both fitting methods since the separation between different particles starts to worsen with TOF. At the momentum of 5 GeV/c the electron purity lies at around 87% / 77% for the standard/template method. For the TPC selection of $-1 < \sigma_{TPC} < 3$ seen in the top right panel of Fig. 3.7 the purity decreases to a value of 30% for both methods, but also here the purity obtained by the standard fit method lies above the purity obtained by the templates. This can be explained by the fact that the templates, since they are obtained from data, are contaminated by other particle species as illustrated in section 3.3, which ill result in an overestimation of the hadron contamination and therefore in a smaller electron purity as seen in Fig. 3.7.

We can therefore come to the following conclusion. First of all, the templates explained in section 3.3 can ideally be used to qualitatively interpret the contriubtions of the differnt hadrons to the contamination of our electron candidates which is not possibly with the standard fit method, because the "background" Gaussian is used to describe the contamination due to protons, kaons and pions at the same time. The template method also helped to understand the content of the cloud seen in the $n\sigma^e_{TPC}$ distribution of the electron candidates and how it contributes to the hadronic contamination of our electron candidates. The standard fit method is more suitable for the estimation of the electron purity and the hadron contamination than the template method is. As seen in section 3.3, the purity of the different templates is heavily dependant on the detector performance and the applied PID selection criteria. Those templates are contaminated by other particles and will therefore lead to an overestimation of the hadron hadron contamination and an underestimation of the electron purity. These problems are avoided by the standard fit routine.

(c) $0 < \sigma^e_{TPC} < 3$ interval
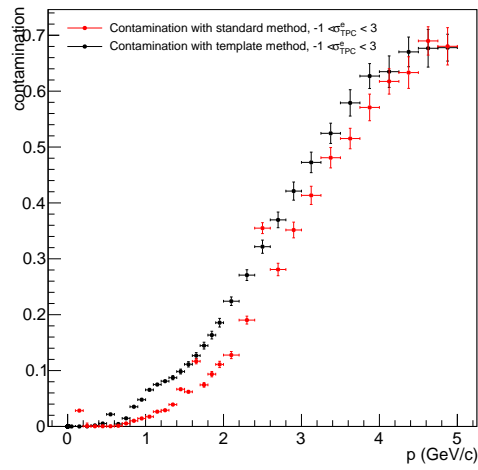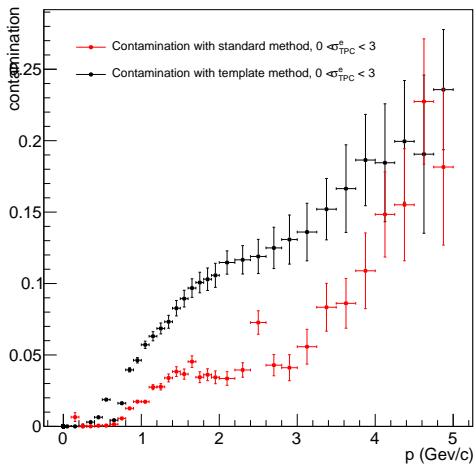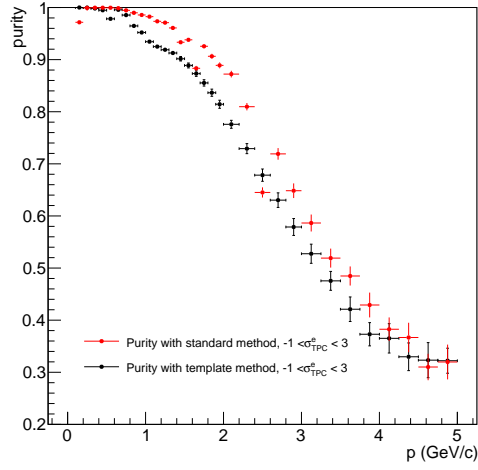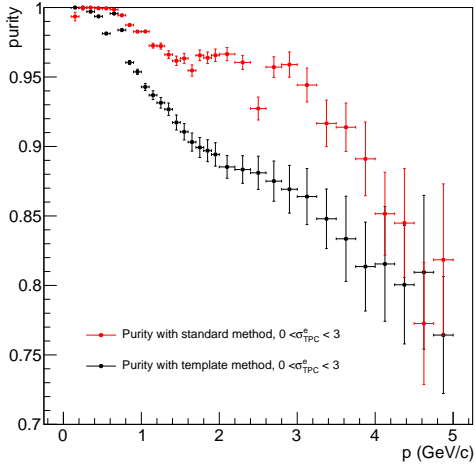
(d) $-1 < \sigma^e_{TPC} < 3$ interval

Figure 3.7: Electron purity and hadron contamination calculated by both fitting methods in the nσ^e_{TPC} interval from 0 to 3 (left) and -1 to 3 (right) for the Pb-Pb data recorded in 2011. The red markers show the purity calculated by the standard fit routine. The black markers show the purity calculated by the template method.

4 Estimtating the electron purity in Pb-Pb collisions at $\sqrt{s} = 5.02\ TeV$ for different fit methods

In the last section two different fit methods were introduced to estimate the electron purity and the hadron contamination of a given electron sample.
The analysis is repeated with a data set of Pb-Pb collisions recorded in 2015 at $\sqrt{s_{NN}}$ = 5.02 TeV in this part of the thesis.

First of all, we check how well the template and standard fit method on the Pb-Pb data recorded in 2015 works compared to the data set of 2011. The differences between most central and peripheral collisions are also investigated.Lastly, the electron purity for different centrality classes with the template and standard fit methods is calculated. In addition the electron purity obtained in this analysis of Pb-Pb collisions recorded in 2015 is compared with the electron purity obtained in the analysis of Pb-Pb collisions recorded in 2011.

4.1 Data Set and track selection

In this part of the thesis Pb-Pb collisions recorded in the year 2015 at a center of mass energy of $\sqrt{s_{NN}}$ = 5.02 TeV are analysed. The analysis concentrates on the most central collisions at 0 - 10%, and more peripheral collisions at 30 - 50% where the total number of 6.4e+06 and 1.4e+07 events were recorded. The track selection criteria, summarized in 3.1, used in this analysis are the same as for the Pb-Pb data set recorded in the year 2011. However, there are some differences and additions compared to the Pb-Pb data recorded in 2011. First of all, an additional cut between the distance of the SPD and the track vertex was applied, leading to a better track signal. One is referred to slide 33 of [26] for more details for the cut. Additionally, it

has to be mentioned that a preliminary TRD parametrization is used in this analysis since a final parametrization was not available at the moment the analysis was done. The data set used in this analysis has a bug in the PID tracking as well, possibly leading to systematic uncertainties which are not investigated further.

4.2 Selection of the electron candidates

The electron candidates for the lead-lead data recorded in 2015 are in the same way obtained like for the data recorded in 2011. First of all, each track has to satisfy the track selection criteria summarized in section 4.1. Then the electron candidates are identified with a selection in TOF in $-2 < \sigma^e_{TOF} < 2$ and a selection in the ITS in $-1 < \sigma^e_{ITS} < 1$ for p < 1.5 GeV/c and $-2 < \sigma^e_{ITS} < 2$ for p $\geq$ 1.5 GeV/c.
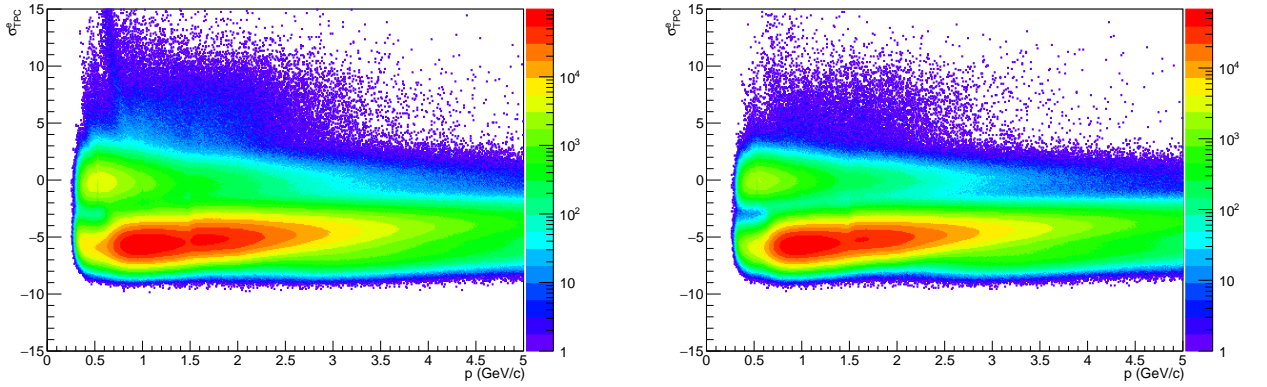

Figure 4.1: nσ^e_{TPC} distribution as function of the momentum for the Pb-Pb data at $\sqrt{s_{NN}} = 5.02$ *TeV* for the centrality classes 0 - 10 % (left panel) and 30 - 50 % (right panel) after TOF and ITS PID described in section 4.2.

Fig. 4.1 shows the electron candidates further analysed in this part for the most central collisions at 0 - 10% centrality in the left panel, whereas for peripheral collisions at 30 - 50% centrality its shown in the right panel after TOF and ITS PID. It is observed that after TOF and ITS PID the kaon and proton bands for the most central collisions are more visible than the ones for peripheral collisions. Moreover, the cloud for the most central events is dominating the nσ^e_{TPC} distribution stronger than for peripheral collisions. The overall hadronic contamination of our electron

candidates seems to be smaller for peripheral events compared to the most central events.

4.3 Template method

The template method used for the Pb-Pb data set recorded in 2011 is applied equally on the electron candidates obtained from the data set of 2015 at the centrality classes of 0 - 10% and 30 - 50%. We will follow the same structure as in section 3.3, but will work out some differences between both data sets.

Fig. 4.2 shows the $n\sigma^e_{TPC}$ distributions for protons (top left panel), pions (top right panel), kaons (bottom left panel) and deuterons (bottom right panel) for the Pb-Pb data set recorded in 2015 at the centrality of 0 - 10%. The $n\sigma^e_{TPC}$ distributions are obtained with the same PID selection criteria in TOF and TRD as for the data set of 2011. As for the electron candidates it can be observed that the contamination of the $n\sigma^e_{TPC}$ distributions for the hadrons, not shown here, in the peripheral collisions are lower than this is the case for more central events.

Additionally, we can compare the $n\sigma^e_{TPC}$ distributions for the hadrons of the 2015 data set (Fig. 4.2) with the 2011 data (Fig. 3.3) at centrality of 0 - 10%. There are no major differences visible for the distributions of protons and deuterons. This is not the case for kaons and pions since the information of the TRD is used on both $n\sigma^e_{TPC}$ distributions. Compared to the kaon distribution of the data set of 2011, the $n\sigma^e_{TPC}$ distribution for kaons from the 2015 data set shows a bigger contamination of pions, electrons and protons. This is also true for the pion $n\sigma^e_{TPC}$ distribution, where a bulge at $n\sigma^e_{TPC} = 0$ is visible at low momenta (below 1.5 GeV/c). This electron contamination is seen better after the projection onto the $n\sigma^e_{TPC}$ for given momentum bin, which will be discussed later.

It's now possible to obtain the templates by projecting the $n\sigma^e_{TPC}$ distributions, described in Fig. 4.2, onto the $n\sigma^e_{TPC}$ for different momentum slices and fit these templates with equation 3.1 to the electron candidates. Fig. 4.3 shows the $n\sigma^e_{TPC}$ distributions fitted via the template method for the low, mid and high momentum regions for the Pb-Pb data set of 2015 at 0 - 10%.
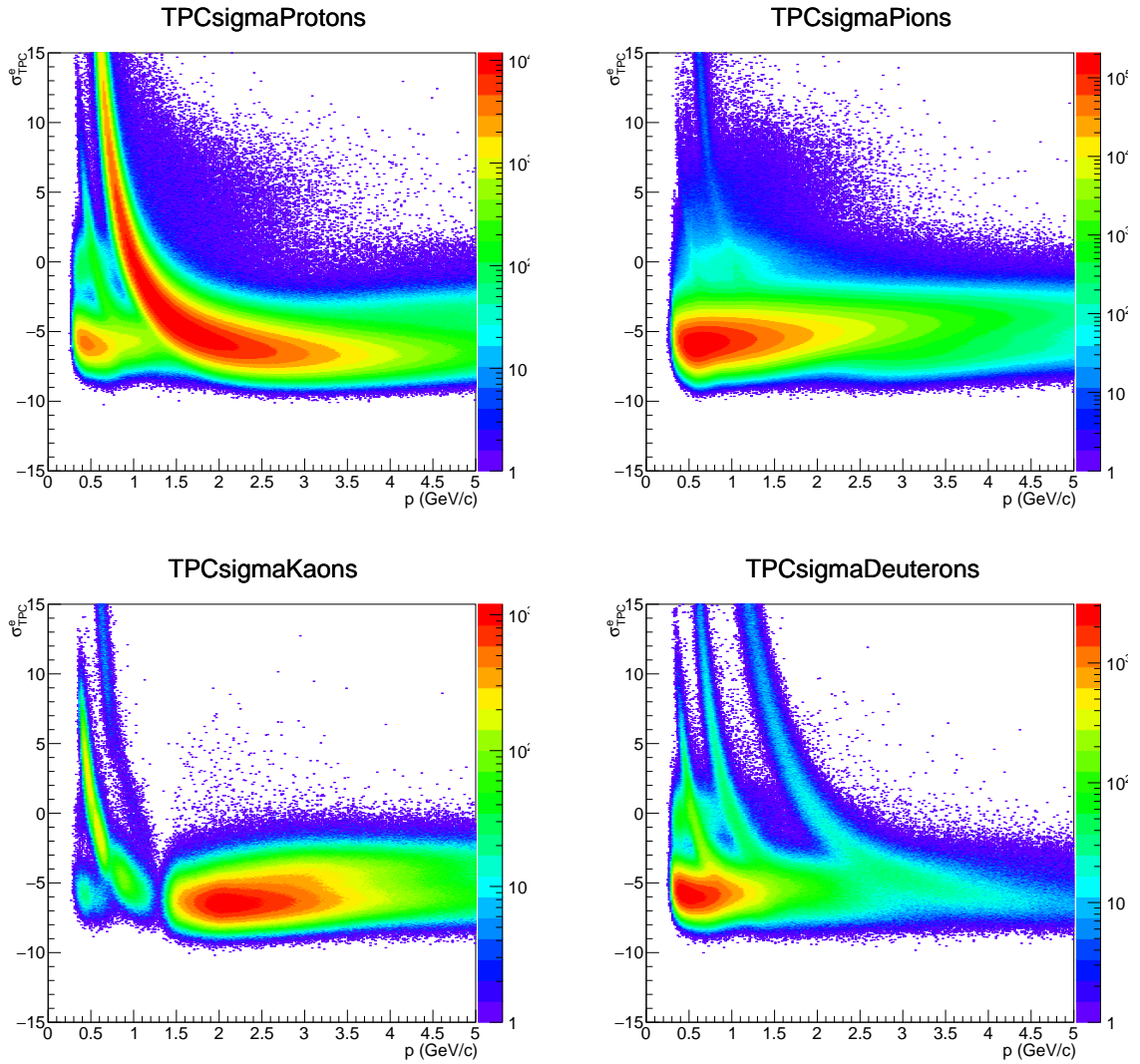
Figure 4.2: nσ_{TPC}^{e} distribution as function of the momentum for protons (top left panel), pions (top right panel), kaons (bottom left panel) and deuterons (bottom right panel) for the Pb-Pb data recorded in the year 2015 at a centrality of 0 - 10%.
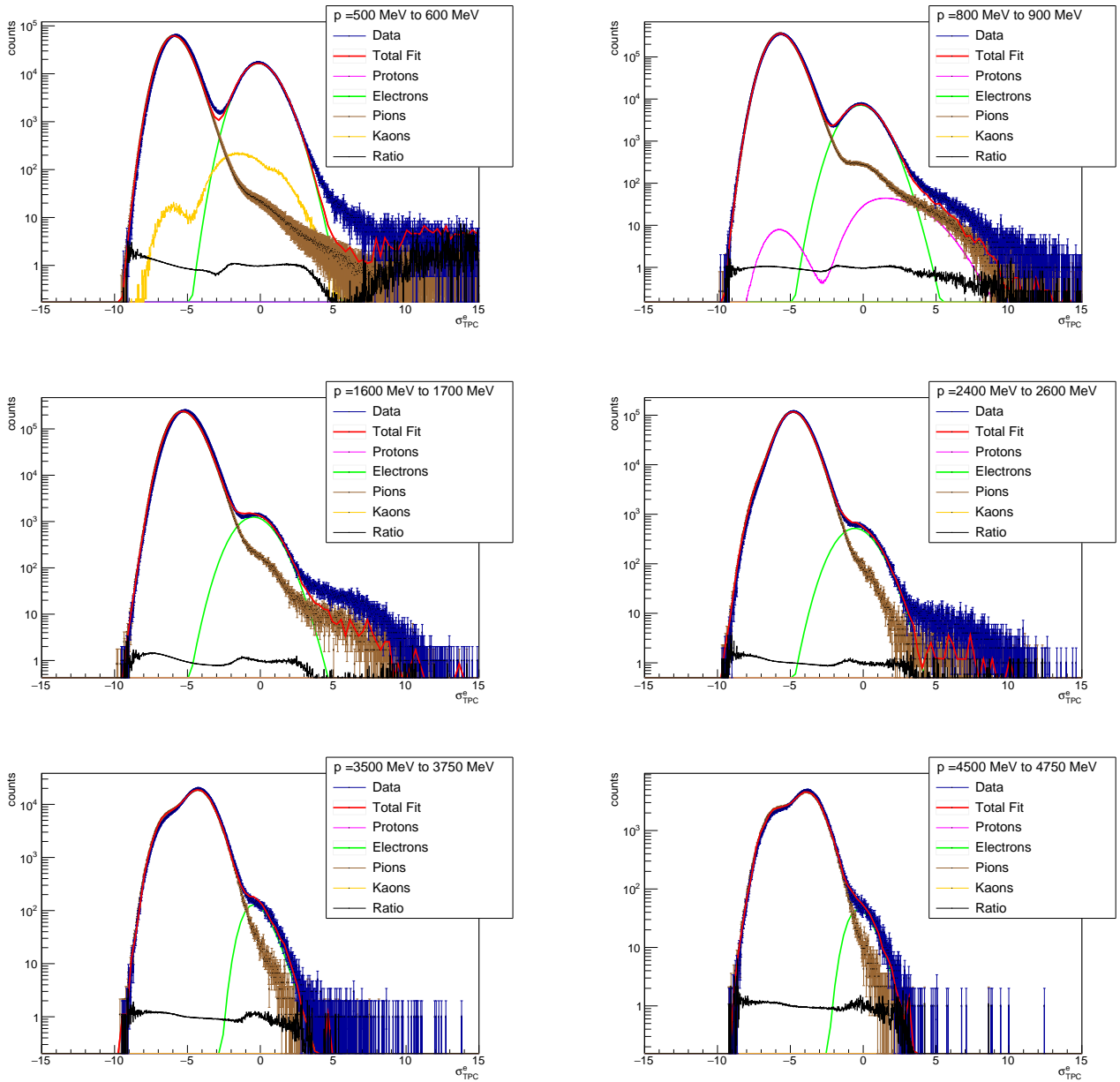
Figure 4.3: Distribution of the $n\sigma^e_{TPC}$ in six different momentum ranges for the Pb-Pb data set recorded in 2015 at centrality 0 - 10%. The distributions are fitted with the fit function in equation (3.1). For high momenta only the pion template is used to explain the hadron contamination.

To allow a better comparison between both data set recorded in 2015 and 2011, Fig. 4.4 shows the p slice for the momentum 0.7 GeV/c to 0.8 GeV/c for both data sets at centrality 0 - 10%, where two observations can be made.
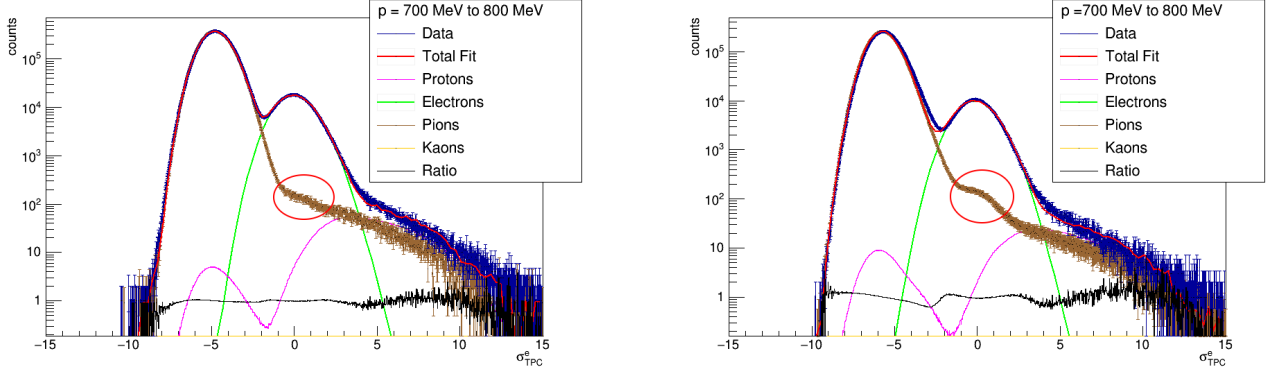

Figure 4.4: Distribution in the $n\sigma^e_{TPC}$ for the momentum p = 0.75 $\pm$ 0.05 GeV/c for the centrality class 0 - 10% for the data recorded in 2011 (left panel) and the data recorded in 2015 (right panel).

First of all, it's visible that the pion template extracted from the data set recorded in 2015 is contaminated by electrons, which is shown by the red circles at σ^e_{TPC} = 0 in Fig. 4.4. This contamination of the pion template due to electrons is observed for the momenta up to 2 GeV/c (see Fig. 4.3). One reason for this larger contamination of the pion template is the preliminary TRD parametrization used in the data set recorded in 2015. Tracks which are actually electrons are more likely identified as pions. This will be crucial for the calculation of the electron purity and lead to an underestimation of the electron purity.

Additionally, one can observe in Fig. 4.5 that the pion template for the 2015 data (right panel) is not capable to describe the shoulder on the left side of the electron peak very well compared to the pion template extracted from the 2011 data set. The ratio (black line) between fit and data is fluctuating much more for the data set of 2015 compared to the one from 2011 in the region of $n\sigma^e_{TPC}$ This observation is also made for the momentum slices in the region of 0.6 - 0.9 GeV/c in 0.1 GeV/c bins.

The same problems for the data of both the centrality class of 0 - 10% and 30 - 50 % can be observed. But as mentioned earlier, the cloud in peripheral collisions is not dominating the electron sample, shown in section 4.1, as much as this is the case for the most central events. The shoulder on the right side of the electron peak

is therefore smaller than for the centrality class of 0 - 10% which is visible in Fig. 4.5. The contamination of the pion template due to electrons is also apparent in the centrality class of 30 - 50%.
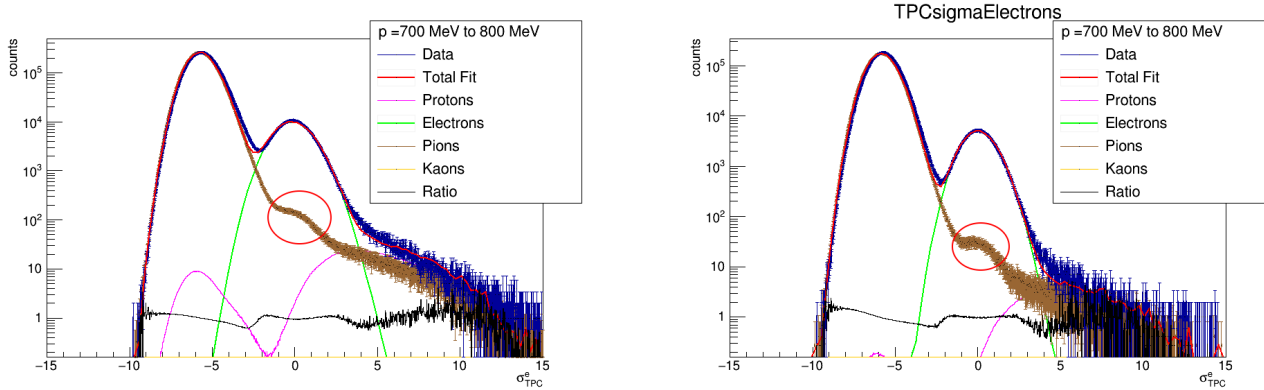

Figure 4.5: Distribution in the $n\sigma^e_{TPC}$ for the momentum region p = 0.75 $\pm$ 0.05 GeV/c for Pb-Pb data recorded in 2015 for the centrality class 0 - 10% (left panel) and 30 - 50% (right panel).

We can therefore conclude that the template method for the data recorded in 2015 does not work as well as for the data set of 2011 which is confirmed by the larger fluctuation of the ratio (black line) beween fit and data in the data set of 2015 (Fig. 4.3) compared to the one of 2011 (Fig. 3.5).

4.4 Standard fit method

The parametrization explained in section 3.4 for the different particle species is applied onto the data recorded in the year 2015 for the different centrality classes for the standard fit routine.

Fig. 4.6 shows the momentum slices in $n\sigma^e_{TPC}$ for the low, mid and high momentum region for the data set recorded in 2015 at the centrality of 0 - 10%. As for the data recorded in 2011, the standard fit routine explains the data overall better than the template method.

All observations and arguments made in section 3.4 for the 2011 data set also applies to the data set recorded in 2015.
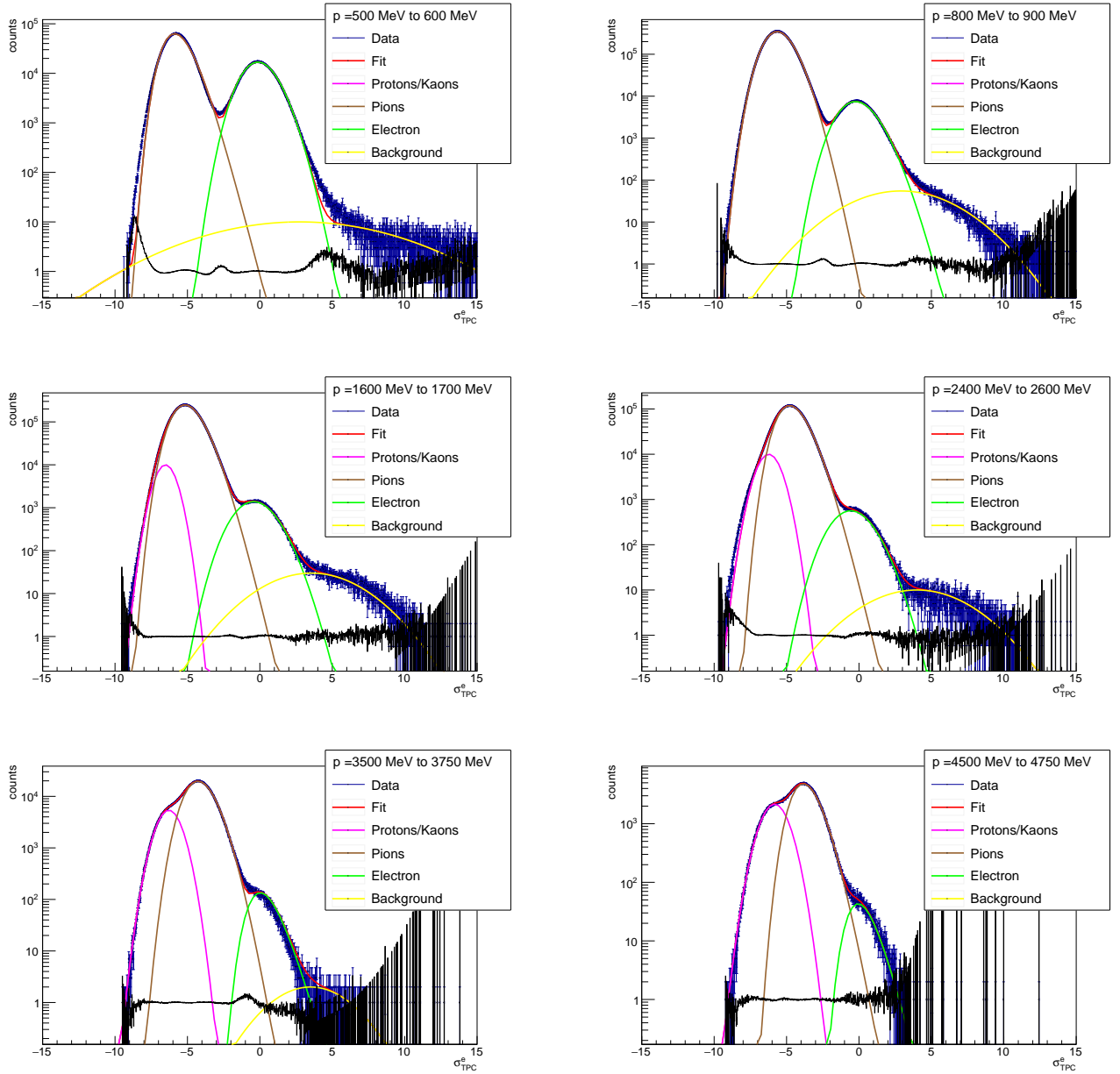
Figure 4.6: Distribution of the $n\sigma^e_{TPC}$ in six different momentum ranges. The distributions are fitted with the fit function described in equation (3.2).

4.5 Electron purity

Both fit methods are now applied to the data set recorded in 2015 for most central collisions and peripheral collisions for the momentum slices in $n\sigma^e_{TPC}$, described in section 3.5. The electron purity is also calculated by the same equations (3.3) - (3.6) outlined in section 3.5 for the $n\sigma^e_{TPC}$ interval from 0 to 3 and -1 to 3.

Fig. 4.7 shows the electron purity for the 2015 data set at 0 - 10% and 30 - 50% centrality in the $n\sigma^e_{TPC}$ interval from 0 to 3 and -1 to 3. As expected, the electron purities obtained by the standard fit routine are higher than the ones from the template method for the data set of 2015 observed for both centrality classes. Additionally, we can identify that a higher electron purity is obtained for the peripheral collisions compared to the more central collisions. This observation can be made by comparing the electron purity for both centrality classes for the fit methods discussed in this thesis.

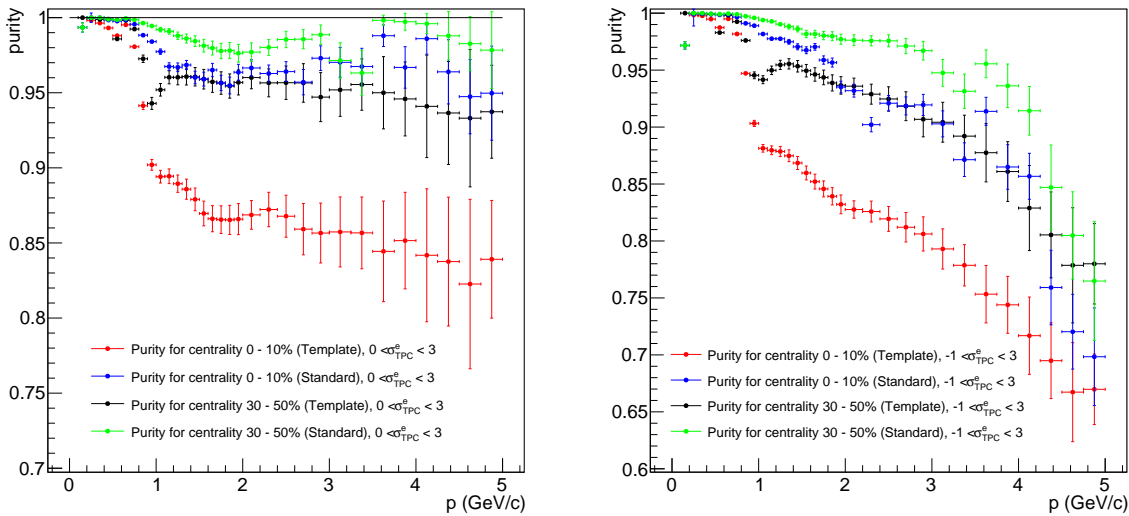Figure 4.7: Electron purity for the data recorded in 2015 at the centrality 0 - 10 % and 30 - 50 % calculated with the template and standard fit method. The left panel shows the electron purity calculated in the $n\sigma^e_{TPC}$ interval from 0 to 3 and the right panel for the $n\sigma^e_{TPC}$ interval from -1 to 3

Moreover, the electron purity obtained for the Pb-Pb data recorded in both 2011

and 2015 can be matched against each other in the n σ^e_{TPC} interval of 0 to 3 and -1 to 3 for most central collisions. Since we have seen in section 4.3 that the template method is not working properly for the Pb-Pb data recorded in 2015, only the electron purity obtained through the standard fit method is compared. The electron purity is comparable within the statistical uncertainties up to a momentum of 3 GeV/c, which is observable for the nσ^e_{TPC}. While the electron purity from the data recorded in 2011 for higher momenta starts to decrease, it continues to be constant within statistical uncertainties in the data from 2015. For higher momenta (bottom two panels of Fig. 4.6) the electron peak better visible in the data set of 2015 compared to the data recorded in 2011 (bottom two panels of Fig. 3.6). In comparision to the data recorded in 2011, this means, there are more electrons in the high momentum slices for the data set of 2015, leading to a higher electron purity, which is also true for the nσ^e_{TPC} interval from -1 to 3. The electron purity is also comparable within the statistical uncertainties up to a momentum of 1.2 GeV/c. The electron purities then start to decrease to a value of 70% (2015 data set) and 30% (2011 data set) for 5 GeV/c.
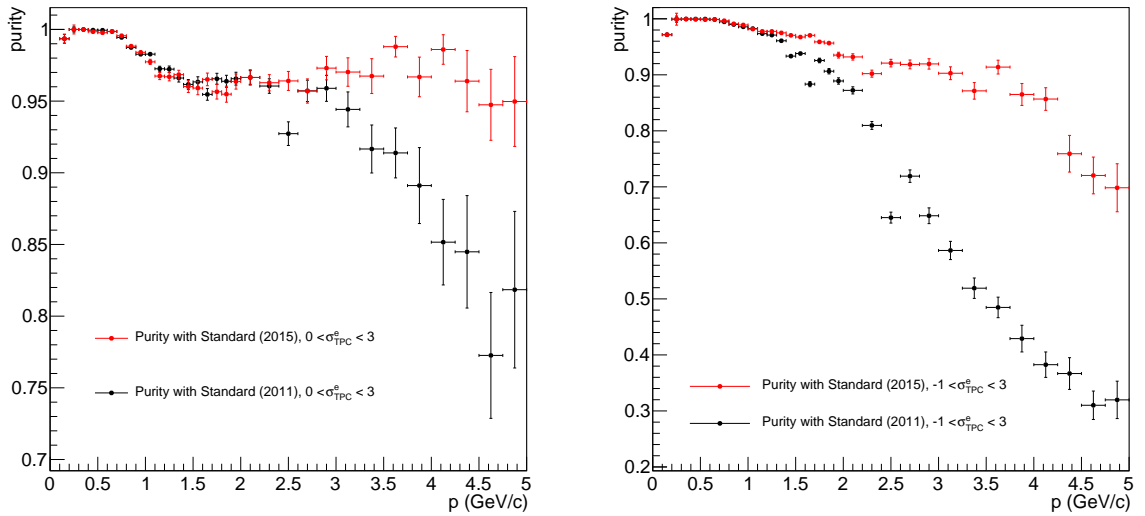

Figure 4.8: Electron purity for the data recorded in 2011 (black markers) and 2015 (red markers) at the centrality 0 - 10% obtained via the standard fit routine in the nσ^e_{TPC} interval of 0 to 3 (left panel) and -1 to 3 (right panel).

5 Estimating the electron purity with TPC and EMCal in proton proton collisions

The electron purity and the hadron contamination of electron candidates was evaluated in the last two section using the ITS, TPC, TOF and TRD detector. While it was possible to perform the analysis up to a momentum of 5 GeV/c with these detectors, higher momenta are out of reach, since the PID capabilities of TOF starts to decrease.

Therefore, a different approach to estimate the electron purity including the higher momenta is explained and discussed in this section of the thesis. Electrons are identified now by the TPC and EMCal detector. The analysis is performed in pp collisions recorded in the year 2011. Additionally, the efficiency of different PID selection criteria is investigated.

5.1 Data Set and track selection

The data analysed in this part of the thesis are pp collisions recorded in 2011 at a center of mass energy of $\sqrt{s}$ = 2.76 TeV. Two different trigger are used in this analysis. For events with transverse momenta below 6 GeV/c the minimum bias trigger, where a hit in one of both VZERO detectors or in the SPD is required, is utilized. The total number of recorded minimum bias events is 2.7e+06. The EMCal trigger, which requires a certain amont of energy above a threshold in a 4 x 4 tower window, is used for events above transverse momenta 6 GeV/c where 1.1e+06 events were recorded. The applied track selection criteria are described in the following.

A minimum of 110 produced clusters in the TPC are necessary for each track, while a minimum of 2 hits, since the SSD layers were not read out in most of the

events out of a maximum of 4, is required in the ITS. We also demand one hit in at least one of the first two layers of the ITS. This guarantees that electrons originate from processes near the vertex and not from pair production because of photons at outer radii. Additionally, this will raise the statistics in our analysis compared to the requirement of a signal in both of the first two layers of the ITS. A cluster in EMCal matching a track from the barrel detectors is needed as well in order to avoid picking up clusters related to neutral particles for which a track is not observed in the TPC. A summary of all track selection criteria applied in this analysis is shown in table 5.1.

description	cut value
No. of TPC clusters	≥ 110
χ^2 per TPC cluster	≤ 4
Require TPC refit	kTRUE
No. of layer hits in ITS	≥ 2
Hit in first two layers	kANY
Require ITS refit	kTRUE
Distance of Closest Approach in xy(cm)	≤ 1
Distance of Closest Approach in z(cm)	≤ 2
Accept kink daughters	kFALSE

Table 5.1: Track selection criteria used in the analysis of the pp data.

Fig. 5.1 shows the TPC dE/dx signal expressed in $n\sigma^e_{TPC}$ after applying the track selection criteria described in table 5.1. The electron band is visible at around σ^e_{TPC} = 0. For high transverse momenta one can observe that hadrons, mainly pions, start to overlap with the electron line coming from the negative σ^e_{TPC}. Therefore, an additional detector is used to reduce the hadronic background at the high transverse momentum region $p_T > 6$ GeV/c and obtain electrons with high purity. The electron identification with the EMCal is explained in the following section.

5.2 Electron identification with the EMCal

Electron identification with the EMCal is based on the measurement of the E/p ratio between the energy deposit in an EMCal cluster E and the matched track momentum p reconstructed in the TPC and ITS detectors. Electrons deposit their total energy in the EMCal and due to their small mass the E/p ratio is close to unity, whereas the
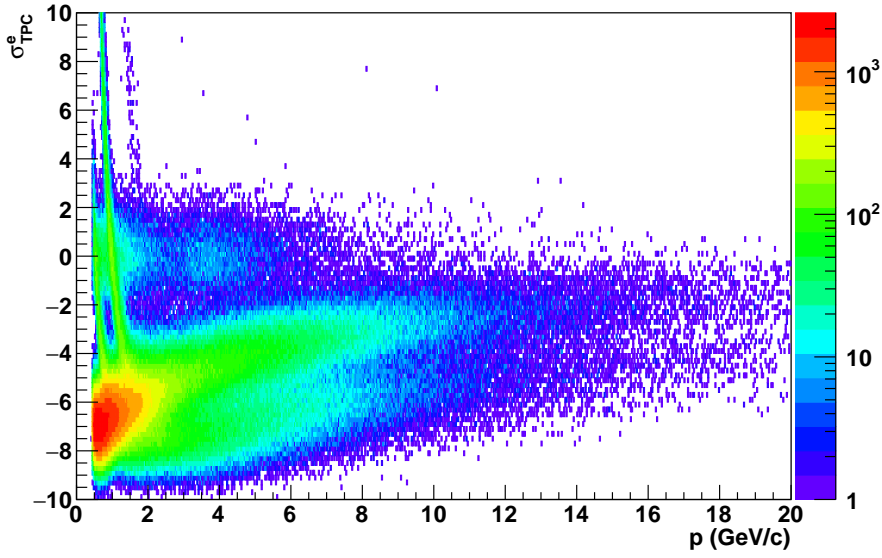
Figure 5.1: nσ^e_{TPC} distribution as function of the momentum for tracks in pp collisions at $\sqrt{s}$ = 2.76 TeV with the criteria summarized in table 5.1.

E/p ratio lies below unity for hadrons. Fig. 5.2 shows the E/p distribution for tracks satisfying the selection in the nσ^e_{TPC} from -3 to 3 (black markers) and -1 to 3 (green markers) for low, mid and high transverse momenta. The electron peak is emerging at E/p equal to unity and the hadrons are seen at low E/p ratios. After a selection of tracks in the nσ^e_{TPC} interval from -3 to 3, we can see the electron peak at E/p equal unity, which is heavily contaminated by the hadronic peak at low E/p, particular for the momentum above 6 GeV/c (mid and right panel in Fig. 5.2). This hadronic background is removed very well after selecting stronger in the nσ^e_{TPC} interval from -1 to 3 (green markers). Even though the stronger nσ^e_{TPC} selection leads to a good rejection of hadrons for the high momentum (right panel), we also observe a starting decrease in statistics. Therefore, an appropriate way to use the EMCal for electron identification, is in selecting tracks within the E/p ratio 0.8 to 1.2.

In order to remove additional hadron contamination an other selection can be applied on the electron candidates. This selection is based on the different shape of the electromagnetic showers between electrons and hadrons in the EMCal detector. It basically consists of selection on the dimension of the short (M20) and long (M02) axis of the transversal projection of the shower [27].
To get an idea of the distribution of the shower shape parameters as function of the
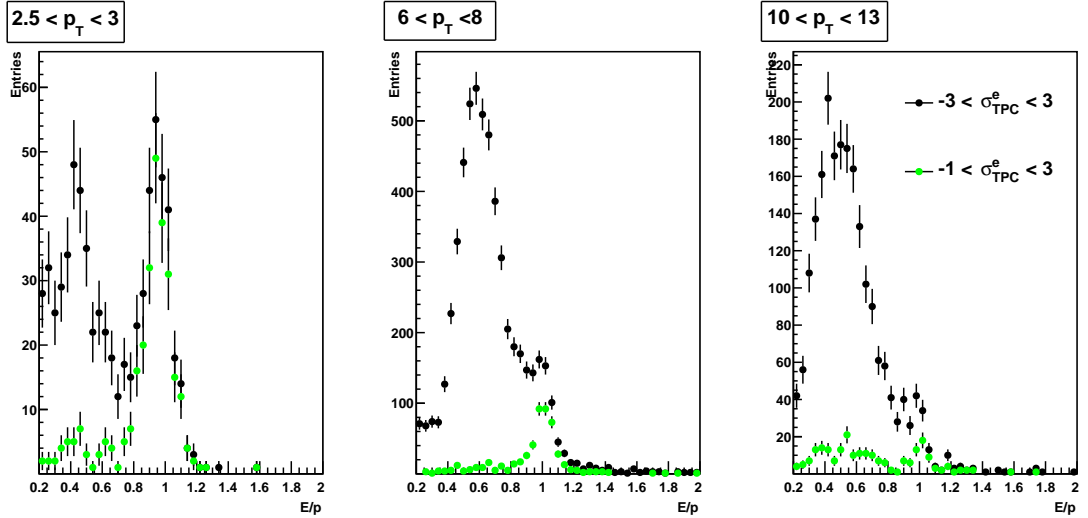
Figure 5.2: Distribution of the E/p for tracks selected in the $n\sigma^e_{TPC}$ interval from -3 to 3 (black markers) and the interval from -1 to 3 (green markers). The three panels show the distributions for tracks in these different regions of transverse momentum.

ratio E/p the TPC is used to identify electrons and hadrons. Fig. 5.3 shows the corresponding distributions for both shower shape parameters for electrons, identified by $-1 < \sigma^e_{TPC} < 3$, and hadrons, identified by $-10 < \sigma^e_{TPC} < -3.5$. On the left side of Fig. 5.3 the electrons are clearly seen at an E/p of around 1. Nevertheless, there are also a lot of hadrons contaminating the tracks selected within $n\sigma^e_{TPC}$ -1 to 3 (right panels in Fig. 5.3). One can therefore suggest cuts to select electrons in M02 around [0.03,0.3] or [0.03, 0.5] and in M20 around [0.03,0.15] or [0.03, 0.3] shown in Fig. 5.3 at the red horizontal lines to identify electrons.

The distributions are only shown for the momenta 2 $GeV/c < p_T < 20$ GeV/c, since the resolution of the calorimeter is proportional to the energy deposit in the EMCal. The energy resolution was measured to be $\sigma_E/E = \sqrt{1.7^2 + 11.3^2/E + 4.8^2/E^2}$ [22]. As a result, the very low p_T region cannot be used for electron identification with the EMCal detector.

The effect of a selection within the shower shape parameter mentioned above on tracks can be investigated furhter by looking at the E/p distributions of tracks which satisfy the selection criteria in M20 and M02. This E/p distributions are shown in Fig. 5.4 for the M02 and Fig. 5.5 for the M20. The black markers in both figures show the E/p distribution for tracks selected in the TPC in the region of -3 to 3 without
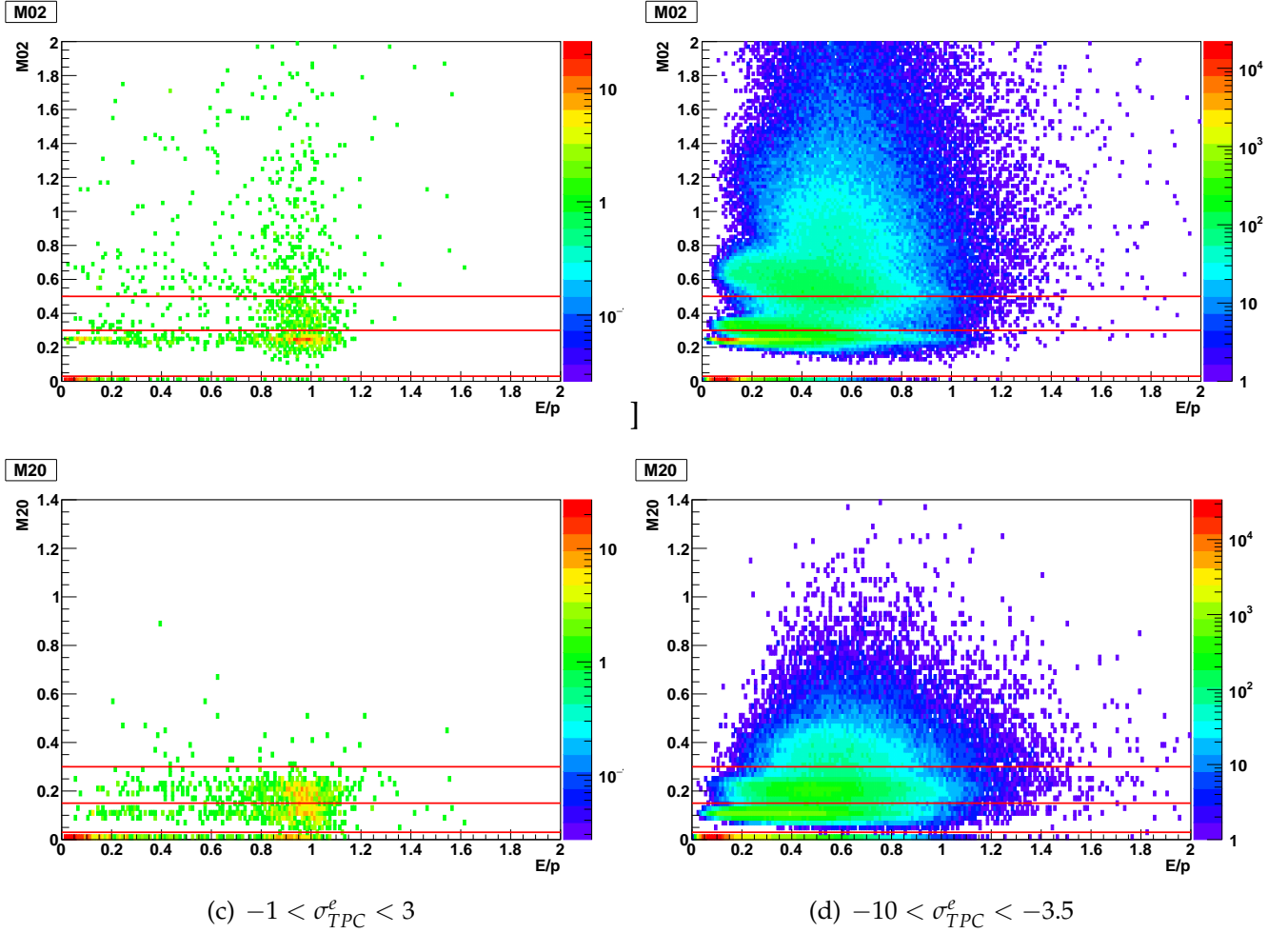
Figure 5.3: Distribution of the shower shape parameters M02 (top two panels) and M20 (bottom two panels) as function of E/p. The left side shows the electrons and the right side shows the hadrons.

any selection in the shower shape parameters. The green/red markers in Fig. 5.4 show the tracks additionally selected in the M20 at around 0.03 to 0.3 and 0.03 to 0.5. One can observe that the M02 cut in the low momentum (left panel) cannot reduce the hadronic background very well. For the mid and high momentum the M02 cuts are rejecting most of the hadrons and preserve the peak emerging at E/p equal to 1, where electrons are expected, to some extend.

Fig. 5.5 shows the E/p distribution for tracks selected in the $n\sigma^e_{TPC}$ interval from -3 to 3 and in the M20 interval from 0.03 to 0.15 (green markers) and 0.03 to 0.3 (red markers). It's observed that the tighter M20 selection (green markers) rejects most of the hadrons, but also a lot of the electrons especially seen in the mid and high

momentum (mid and right panel). Although a loose selection in M20 results in a higher electron peak, many hadrons will remain.

Nevertheless a selection in the M20 or M02 can lead to further selection of hadrons in addition to a selection in the $n\sigma^e_{TPC}$ of the TPC.
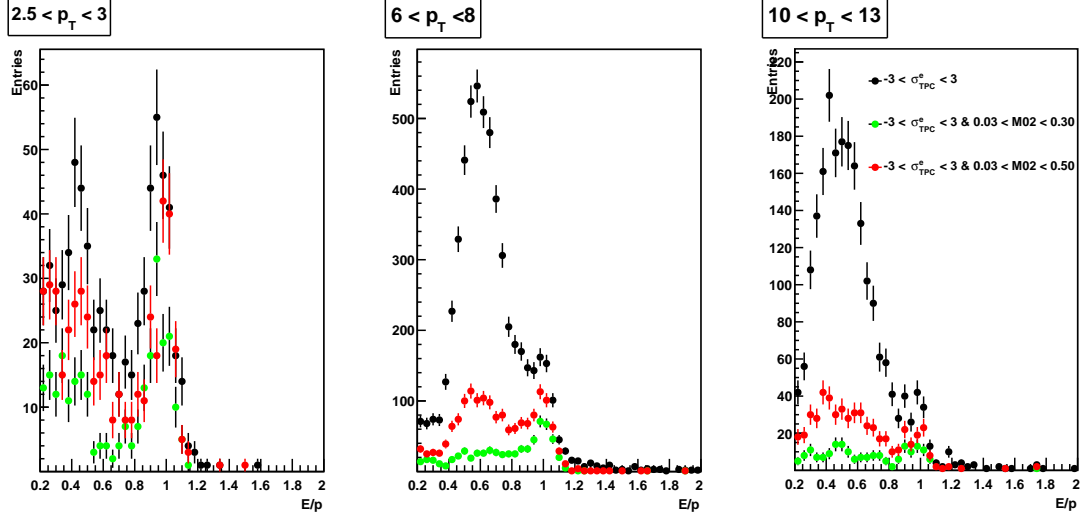

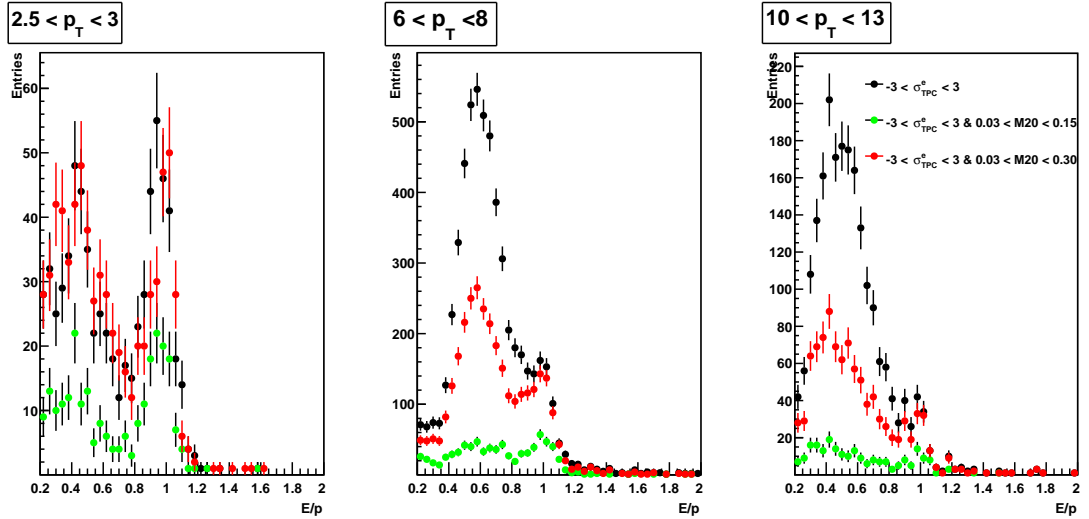Figure 5.4: Distributions for E/p for different momentum slices and different selections in the M02.

Figure 5.5: Distributions for E/p for different momentum slices and different selections in the M20.

5.3 Signal and background extraction

In order to remove the remaining hadron contamination from our electron sample, obtained after the selection in the TPC or the shower shape as explained in the last section, we also derive the E/p distribution (shown for example in Fig. 5.4) for hadrons, selected within the $n\sigma_{TPC}^{e}$ interval of -10 to -3.5. Additionally, the hadronic sample has to satisfy the same PID cuts as the electron sample. The E/p distributions of the tracks selected as hadrons are now scaled to the ones selected by the TPC, M20 or M02 for each p_T bin to the region of low E/p values (0.2 < E/p < 0.45). Fig. 5.6 shows this process of signal and background extraction. In the left panel of Fig. 5.6 a good agreement between the E/p distributions for the electron candidates (black markers) and for the scaled hadrons (magenta markers) for the region left to the electrons is observed. A "pure" electron sample (blue markers right panel) can now be obtained by subtracting the scaled hadron background from the electron sample. Nevertheless, an oversubstraction of the hadronic background in the region of E/p = 0.6 to 0.8 can be noticed on the right panel of Fig. 5.6. This overestimation of the hadronic background in the region of E/p 0.6 could also lead to one in the E/p region from 0.8 to 1.2, where the electrons are located, as well, resulting in an undervaluation of the electron purity which has to be taken into account.
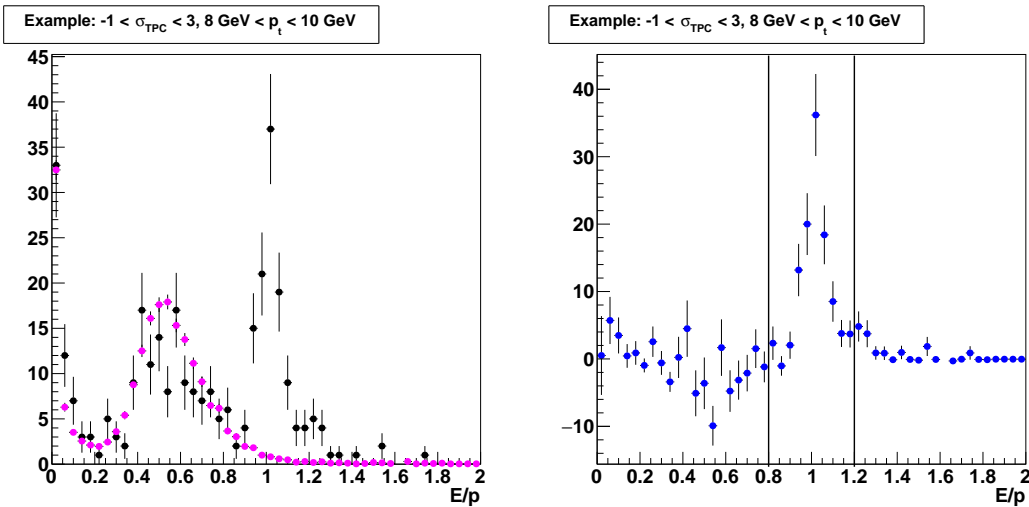

Figure 5.6: Scaled hadronic sample, selected in the $n\sigma_{TPC}^{e}$ interval of -10 to -3.5, (magenta) and electron sample, selected in the $n\sigma_{TPC}^{e}$ interval of -1 to 3, (black) for the transverse momentum 8 GeV/c to 10 GeV/c. The right panel shows the "pure" electron sample, obtained by subtracting the two samples in the left panel.

5.4 Trigger efficiency

The EMCal trigger extends our analysis to high p_T for electrons and will sum the deposited energy in a 4 x 4 tower window. If the energy exceeds a certain threshold, a event is selected by the trigger. Since the EMCal trigger only selects certain events, effectively enhancing the statistics in the higher p_T region above the trigger threshold, the cross section involved in these processes are naturally different than compared to a minimum bias spectrum [27]. However, the bias introduced by the use of an event trigger is not directly relevant here because this analysis concentrates on electron identification. Nevertheless, it is important to know the threshold above which the track from triggered data can be used, and the enhancement factor that implicates the increase of the number of tracks from triggered data compared to minimum bias trigger data. Both quantities are described and estimated in the following.
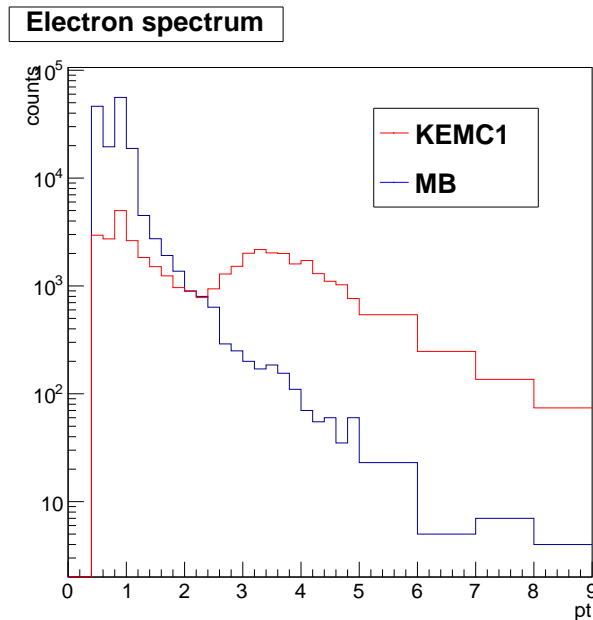
Figure 5.7: Electron spectrum as function of p_T for EMCal trigger and minimum bias events. Note that the spectrum is normalized to the bin size.

The relative trigger efficiency[1] is estimated through reconstructing the ratio of the p_T spectrum of electrons derived from both EMCal trigger data and minimum bias

---

[1]This is an arbitrary name for the calculated ratio between EMCal trigger data and minimum bias data. The trigger efficiency has values between 0 and 1 in many analyses, being one for tracks above the trigger threshold.

data. In both cases the electron sample is obtained by selecting in the $n\sigma^e_{TPC}$ interval from -1 to 3 and E/p interval from 0.8 to 1.2 in the EMCal. Fig. 5.7 shows the electron spectrum as function of p_T, normalized to the bin size, for the EMCal trigger and minimum bias data. The number of electrons from the minimum bias data starts to heavily decrease for transverse momenta above 5 GeV/c

Fig. 5.8 shows the ratio of both trigger data as a function of the transverse momentum p_T. While the ratio starts to rise with increasing momenta up to p_T = 5 GeV/c, it stagnates and stays constant within statistical fluctuations. The starting point of the plateau corresponds to the searched threshold and is estimated to be at $p_T \approx 5$ GeV/c according to visual judgement. The enhancement factor is derived by the ratio at the plateau. A constant function is fitted on the plateau illustrated as a black line in Fig. 5.8. The enhancement factor is calculated to be $\epsilon_{Trigger}$ = 24.1 ± 2.2. However, the obtained results are not very stable and fluctuate due to limited statistics at high transverse momenta for the bias data shown in Fig. 5.7.
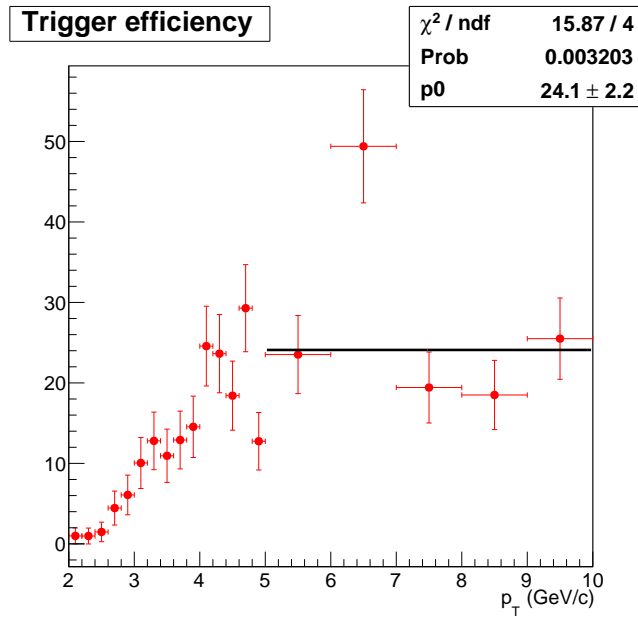
Figure 5.8: Relative trigger efficiency determined with the transverse momentum p_t of the full track

A second method to calculate the relative trigger efficiency is used and compared to the first one. Instead of considering the transverse momentum spectra of electrons, we study the ratio as a function of the electron cluster energy. [28]. The electron spectrum is obtained with the same selection criteria as for the p_T spectrum. The derived ratio

is seen in Fig. 5.9. Up to an energy of E = 5 GeV a rise in the ratio with increasing energy is observed, whereas a constant ratio for high energies E is witnessed. As before, the enhancement factor is calculated by fitting a constant function to the data above the threshold E $\approx$ 5 GeV. The enhancement factor is calculated to be $\epsilon_{Trigger}$ = 25.1 $\pm$ 2.2. Compared to the p_T spectrum a more stable result is obtained. The threshold and enhancement factor obtained by both methods are in good agreement with each other within statistical uncertainties.
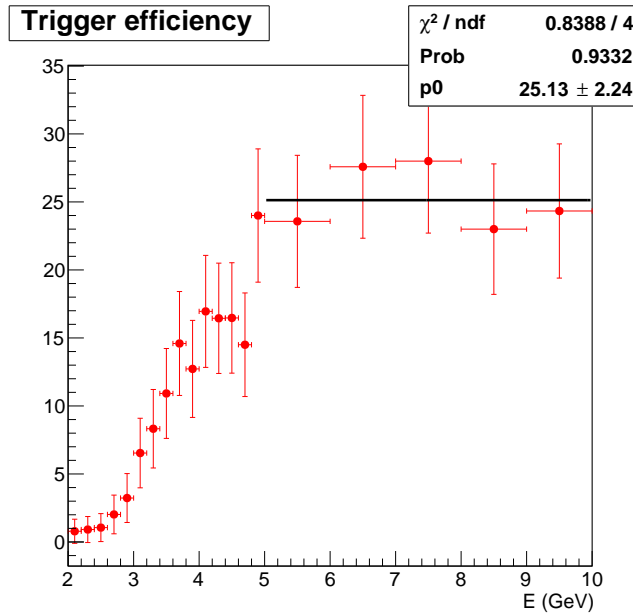
Figure 5.9: Relative trigger efficiency determined with energy deposit in the EMCal cluster.

We can therefore conclude that the EMCal trigger data is only used for transverse momenta above 6 GeV/c because it guarantees the data is only applied in the region of the plateau. Other than that, the minimum bias data is used.

5.5 Electron purity and efficiency

With the considerations in the last three sections, the purity and efficiency of an electron sample for different momentum slices in the region of 2 GeV/c to 13 GeV/c are derived. The purity is calculated by the following equation:

$$P = \frac{N_e}{N_e + N_{Hadrons}} \tag{5.1}$$

where N_e is obtained by integrating the electron sample, as explained in section 5.3 and shown in Fig. 5.6 (blue markers, at right panel) over the E/p interval from 0.8 to 1.2, whereas $N_{Hadrons}$ is obtained through integration of the scaled hadronic sample (magenta markers in Fig.5.6) at the same E/p interval.

$N_{Hadrons}$ is on the other hand obtained by integrating the scaled hadronic sample (magenta markers in Fig. 5.6) in the E/p interval from 0.8 to 1.2.

The efficiency for different PID cuts is derived by:

$$E = \frac{N_{withcuts}}{N_{withoutcuts}} \tag{5.2}$$

$$E_{SS} = \frac{N_{SS+TPC}}{N_{TPC}} \tag{5.3}$$

Equation (5.3) is used when the electron sample is obtained by selecting in the shower shape parameters, while the TPC PID is not used at all. N_{TPC+SS} is aquired by integrating the sample of tracks, satisfying a given selection in the shower shape and in the $n\sigma^e_{TPC}$ from -1 to 3, in the E/p interval from 0.8 to 1.2, whereas N_{TPC} only describes the integrated sample after selection in $n\sigma^e_{TPC}$ from -1 to 3. Since the TPC selection is used in both the nominator and denominator of eq. (5.3), it cancels each other out and only the effect of the chosen shower shape parameter on the efficiency is taken into account. The efficiency for the shower shape cuts are calculated in this way, since the shower shape distributions are not well reproduced in Monte Carlo simulations. This data driven method is therefore chosen, while eq. (5.2) is used for the other cuts investigated below.

The purity and efficiency for different PID cuts are seen in Fig. 5.10. In the top two panels the purity and efficiency are calculated after applying different strong cuts to the $n\sigma^e_{TPC}$. Both purity and efficiency for different selections in the M02 and M20, without using the TPC PID information, is illustrated by the middle and bottom panels.

As expected, the purities for different TPC cuts are dropping for increasing transverse momenta. This effect is stronger for weaker selections in $n\sigma^e_{TPC}$, since at negative $n\sigma^e_{TPC}$ hadrons, mainly pions, will be selected to the sample and contaminate it. The efficiency for the TPC cuts $0 < \sigma^e_{TPC} < 3$ and $-1 < \sigma^e_{TPC} < 3$ in the low momenta are

approximately 0.5 / 0.9, which are in good agreement with the efficiency calculated by using only the TPC, following the expected Gaussian distribution when the TPC dE/dx signal is converted to a $n\sigma^e_{TPC}$ signal as explained in section 2.6.

A rise in purity is observed for cuts in M02, while the efficiency stays roughly constant over a large momentum region. It can also be monitored that tighter cuts in the M02 result in higher purities and an expected drop in efficiency, since tighter cuts decrease the electron signal. A higher purity is also anticipated since hadronic contamination is removed by M02 cuts very well, as shown in Fig. 5.4. The same shape of purity and efficiency is observed for the M20 shower shape parameter, but with a general higher efficiency compared to the M02 cuts.

Comparing the purity and efficiency of both the M20 and TPC cuts leads to the conclusion, that the shower shape parameters are no real alternative to a cut in the TPC. The purity obtained by cutting in $-1 < \sigma^e_{TPC} < 3$ is much higher than the one obtained by cutting in the shower shape parameters. However, the efficiency for different M02 cuts for the high momentum region lies above the efficiency attained by a selection in the $n\sigma^e_{TPC}$ interval from -1 to 3. For a comparison of both TPC and M20 cuts the same arguments apply as well.
In order to obtain electron samples with high purity a combination of TPC and M20 is analysed. The purity and efficiency for the combination of PID cuts are shown in Fig. 5.11. A rise in electron purity by using an additional cut in the shower shape parameter M20 compared to only selecting in the TPC can indeed be observed, but lead to a drop in efficiency since adding an additional PID cut to the TPC cut also reduces the statistics of our sample

We an therefore conclude that a TPC cut combined with a E/p cut at around 0.8 < E/p < 1.2 is the best way to extend the analysis to transverse momenta above 5 GeV/c obtain enough statistics while having a high electron purity. Selections in the shower shape parameters M20 and M02 show potential in being a possible alternative at higher momenta, but the use of shower shape parameters can be excluded for the data sample of pp collisions analysed in this part of the thesis. Also a combination of TPC and shower shape is excluded, since the gain in purity cannot compensate the reduction in statistics by using additional PID cuts. This for example is not the case for Pb-Pb data, since here a higher particle multiplicity is measured and therefore an
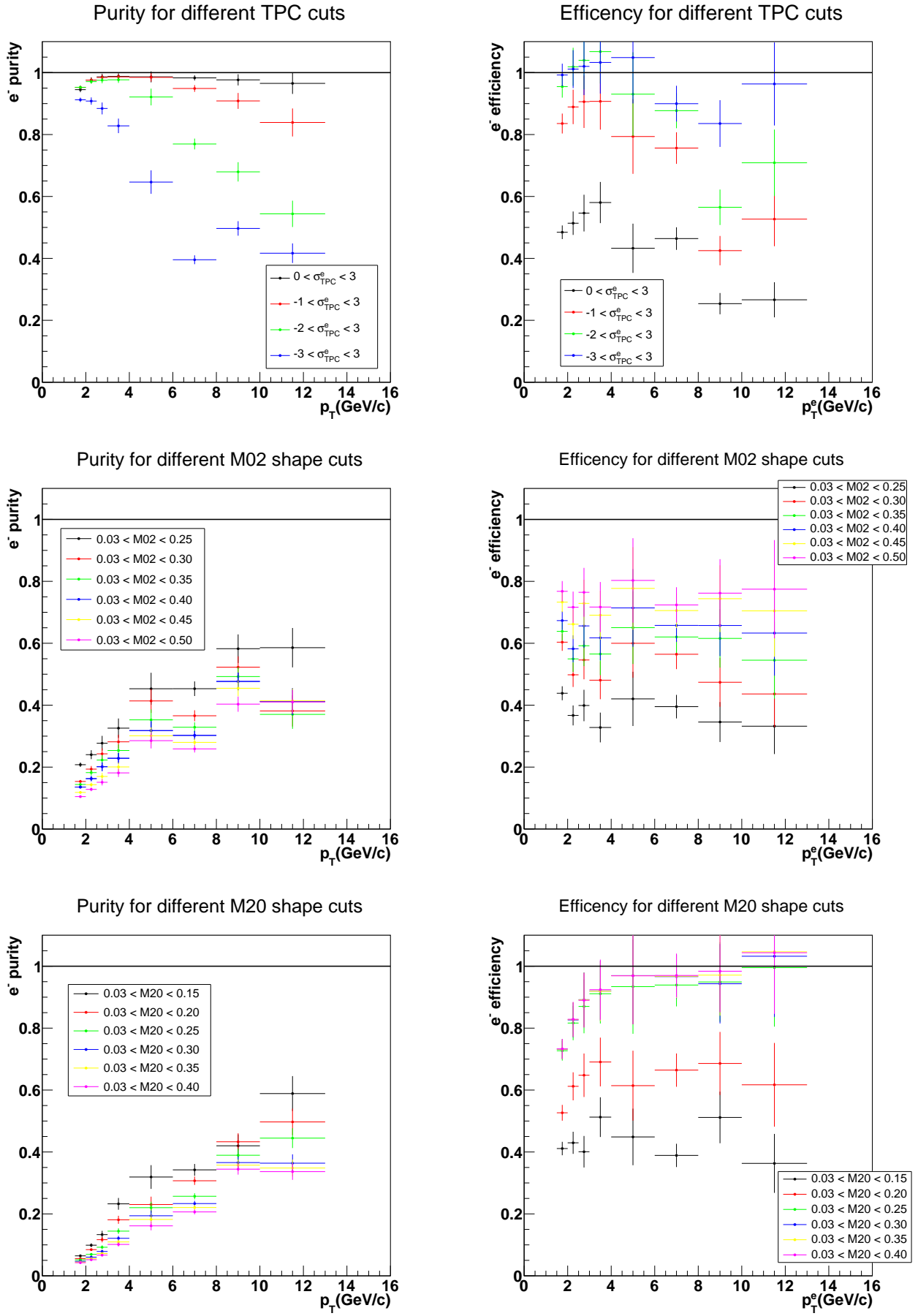
Figure 5.10: Purity (left panel) and efficiency (right panel) obtained after selection in the TPC (top two panels) and the the shower shape parameter M02 (mid two panels) and M20 (bottom two panels)
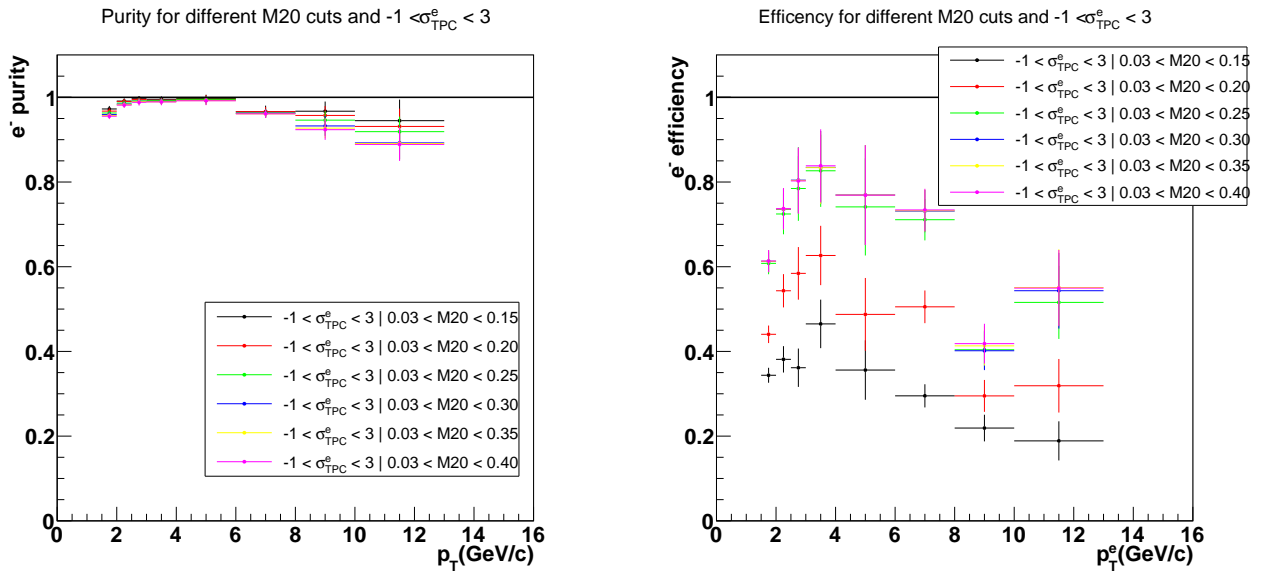
Figure 5.11: Purity (left panel) and Efficiency (right panel) obtained after selection in TPC and M20.

additional selection in the shower shape can help to obtain electrons with high purity. The same is true for pp collisions at higher center of mass energy.

6 Summary and Outlook

In this bachelor thesis the electron purity and the hadron contamination was estimated in two different colliding systems with different detectors of the ALICE experiment. In the sections 3 and 4 an estimation of the electron purity and hadron contamination for Pb-Pb data recorded in the year 2011 and 2015 at a center of mass energy of 2.76 TeV and 5.02 TeV was given with ITS, TOF, TPC and TRD. The estimation of the hadronic contamination was done by fitting two different fit methods to the data set of the electron candidates. While the different particles were described by so called templates extracted directly from the data in a first approach they were described by different functions in a second approach.

Those templates or functions were then scaled to several momentum slices in $n\sigma^e_{TPC}$ of our electron sample and made an estimation of the electron purity over the momentum interval from 0 GeV/c to 5 GeV/c in the $n\sigma^e_{TPC}$ interval from 0 to 3 and -1 to 3 possible. The results of this part of the analysis is shown in Fig. 3.7 for the data recorded in 2011 and in Fig. 4.7 for the data recorded in 2015 for different centrality classes. Fig. 4.8 compares the electron purity obtained from both the data set recorded in 2011 and 2015 with each other.

We could observe a higher electron purity with the standard fit method compared to the template method for both data sets, which was expected since the templates are extracted from measured dE/dx distributions that are contaminated by other particles, resulting in an underestimation of the electron purity. The template method allowed for a qualitative description of the contamination nevertheless, whereas the standard fit method id better for a quantitative estimation of the electron purity.

However, some improvements could possibly be made especially for the data recorded in 2015. First of all, the analysis of the Pb-Pb data recorded in 2015 must be redone with a more advanced TRD parametrization, since the TRD information is crucial for the pion template. Additionally, one has to investigate the effect of the bug in the PID tracking on the templates, electron purity and contamination on the

other hand, which can be done by repeating the analysis with data where no bug was observed. Since a list without the PID tracking bug exists for Pb-Pb data recorded in 2015, the electron purity analysis can be redone for the data with and without the bug in order to be able to evaluate its impact.

In section 5 of the thesis the electron purity was estimated with the TPC and EMCal for a sample, obtained from pp data recorded in 2011 at a center of mass energy of 2.76 TeV. The hadronic contamination was measured through selecting electron candidates within a $n\sigma_{TPC}^e$ region or a interval in the two shower shape parameters M20 and M02 first, followed by a selection of hadrons with the TPC in the $n\sigma_{TPC}^e$ from -10 to -3.5. The hadronic sample was then scaled to the selected electrons in the E/p region below 1, where mainly hadrons are excepted. This allowed us to estimate the electron purity of the selected electron candidates for the E/p interval from 0.8 to 1.2. The results of this analysis for different PID selection criteria in TPC and EMCal are shown in Fig. 5.10 and 5.11. We could conclude that the use of a selection in the shower shape parameters could be excluded and only the use of the TPC in combination of the selection in the E/p with the EMCal allows to obtain high electron purities with relatively high statistics.
We observed a lack of statistics for transverse momenta above 6 GeV/c for the pp data at the center of mass energy of 2.76 TeV, making a presice calculation of the electron purity at high momenta difficult.

The analysis represented in this thesis could therefore be repeated for pp collisions at a higher center of mass energy, where a higher average multiplicity is expected and therefore a rise in the statistics at high p_T. Lastly, one can redo the analysis with Pb-Pb collisions where the overall hadronic contamination is higher which is why additional shower shape cuts can held to reduce the hadronic contamination further. Additionally, the electron purity obtained in the analysis of Pb-Pb collisions with TPC and EMCal, presented in section 5, can then be compared with the results one obtain with ITS, TOF, TPC and TRD, presented in section 3.

Bibliography

[1] R. Averbeck. Heavy-flavor production in heavy-ion collisions and implications for the properties of hot QCD matter. *Prog. Part. Nucl. Phys.*, 70:159–209, 2013.

[2] Rajeev S Bhalerao. Relativistic heavy-ion collisions. (arXiv:1404.3294):21 p, Apr 2014.

[3] J. Schukraft. Heavy Ion physics with the ALICE experiment at the CERN LHC. *Phil. Trans. Roy. Soc. Lond.*, A370:917–932, 2012.

[4] A. Bazavov et al. Equation of state in (2+1)-flavor QCD. *Phys. Rev.*, D90:094503, 2014.

[5] P. Braun-Munzinger, A. Kalweit, K. Redlich, and J. Stachel. Confronting fluctuations of conserved charges in central nuclear collisions at the LHC with predictions from Lattice QCD. *Physics Letters B*, 747:292 – 298, 2015.

[6] A. Andronic. The study of quark-gluon matter in high-energy nucleus-nucleus collisions. *AIP Conf. Proc.*, 1498:125–133, 2012.

[7] Federico Antinori and Urs Wiedemann. ALICE: Physics Performance Report, Volume II. *Journal of Physics G: Nuclear and Particle Physics*, 32(10), 2006.

[8] R. Baier, Yuri L. Dokshitzer, Alfred H. Mueller, S. Peigne, and D. Schiff. Radiative energy loss of high-energy quarks and gluons in a finite volume quark - gluon plasma. *Nucl. Phys.*, B483:291–320, 1997.

[9] K Nakamura and Particle Data Group. Review of Particle Physics. *Journal of Physics G: Nuclear and Particle Physics*, 37(7A):075021, 2010.

[10] The ALICE Collaboration. The ALICE experiment at the CERN LHC. *Journal of Instrumentation*, 3(08):S08002, 2008.

[11] Lyndon Evans and Philip Bryant. LHC Machine. *Journal of Instrumentation*, 3(08):S08001, 2008.

[12] Betty Bezverkhny Abelev et al. Performance of the ALICE Experiment at the CERN LHC. *Int. J. Mod. Phys.*, A29:1430044, 2014.

[13] Yvonne Pachmayer. Physics with the ALICE Transition Radiation Detector. 2011. [Nucl. Instrum. Meth.A706,6(2013)].

[14] ALICE Collaboration, F Carminati, P Foka, P Giubellino, A Morsch, G Paic, J-P Revol, K Safarík, Y Schutz, and U A Wiedemann. ALICE: Physics Performance Report, Volume I. *Journal of Physics G: Nuclear and Particle Physics*, 30(11):1517, 2004.

[15] Deepa Thomas and Andre Mischke. *Jet-like heavy-flavour particle correlations in proton-proton and lead-lead collisions in ALICE*. PhD thesis, Utrecht U., Apr 2014. Presented 16 Jun 2014.

[16] L. Milano. Transverse momentum spectra of hadrons identified with the ALICE Inner Tracking System. In *Proceedings, Physics at LHC 2011: International Conference held in Perugia, Italy, June 6-11, 2011*, 2013.

[17] J. Alme, Y. Andres, and H. Appelshäuser et al. The ALICE TPC, a large 3-dimensional tracking device with fast readout for ultra-high multiplicity events. *Nuclear Instruments and Methods in Physics Research Section A: Accelerators, Spectrometers, Detectors and Associated Equipment*, 622(1):316 – 367, 2010.

[18] Url: http://aliceinfo.cern.ch/public/en/chapter2/chap2_tof.html (zugriff am 9.12.2016).

[19] Christian Lippmann. Particle identification. *Nucl. Instrum. Meth.*, A666:148–172, 2012.

[20] URL: http://aliceinfo.cern.ch/Public/en/Chapter2/Chap2_TRD.html (zugriff am 9.12.2016).

[21] Xian-Guo Lu. Energy Loss Signals in the ALICE TRD. *Nucl. Instrum. Meth.*, A706:16–19, 2013.

[22] U. Abeysekara et al. ALICE EMCal Physics Performance Report. 2010.

[23] Mark T Heinz and the ALICE collaboration. Heavy flavor measurements using high- p T electrons in the ALICE EMCal. *Journal of Physics: Conference Series*, 230(1):012005, 2010.

[24] Podist Kurashvili. Photon and neutral pion production in pp and Pb-Pb collisions at LHC energies in the ALICE experiment. In *International School on High Energy Physics: Session C: Workshop in HEP (LISHEP 2015) Manaus, Amazonas, Brazil, August 2-9, 2015*, 2015.

[25] Jaroslav Adam et al. Particle identification in ALICE: a Bayesian approach. *Eur. Phys. J. Plus*, 131(5):168, 2016.

[26] C. Zampolli F. Prino. Update on 5 TeV Pb+Pb processing and analysis guidelines. 5 October 2016.

[27] Tomas Robert Prem-Raj Aronsson. *Cross section of bottom electrons in proton-proton collisions in the ALICE experiment*. PhD thesis, Yale University, 2014.

[28] Deepa Thomas Bernard Hicks. Analysis Note: Electrons from Semi-Leptonic Heavy-Flavor Hadron decays in pp collisions at sqrt(s) = 2.76 TeV. July 2012.

Erklärung

Ich versichere, dass ich diese Arbeit selbstständig verfasst und keine anderen als die angegebenen Quellen und Hilfsmittel benutzt habe.

Heidelberg, den 14. Dezember ,